



Loss of the Extracellular Matrix Molecule Tenascin-C Leads to Absence of Reactive Gliosis and Promotes Anti-inflammatory Cytokine Expression in an Autoimmune Glaucoma Mouse Model

OPEN ACCESS

Edited by:

Kim Midwood,
University of Oxford, United Kingdom

Reviewed by:

Martin Degen,
Universität Bern, Switzerland
Anna Maria Piccinini,
University of Nottingham,
United Kingdom

*Correspondence:

Stephanie C. Joachim
stephanie.joachim@rub.de
Andreas Faissner
andreas.faissner@rub.de

†These authors have contributed
equally to this work

Specialty section:

This article was submitted to
Inflammation,
a section of the journal
Frontiers in Immunology

Received: 27 May 2020

Accepted: 26 August 2020

Published: 09 October 2020

Citation:

Wiemann S, Reinhard J, Reinehr S,
Cibir Z, Joachim SC and Faissner A
(2020) Loss of the Extracellular Matrix
Molecule Tenascin-C Leads to
Absence of Reactive Gliosis and
Promotes Anti-inflammatory Cytokine
Expression in an Autoimmune
Glaucoma Mouse Model.
Front. Immunol. 11:566279.
doi: 10.3389/fimmu.2020.566279

Susanne Wiemann¹, Jacqueline Reinhard¹, Sabrina Reinehr², Zülal Cibir¹,
Stephanie C. Joachim^{2*†} and Andreas Faissner^{1*†}

¹ Department of Cell Morphology and Molecular Neurobiology, Faculty of Biology and Biotechnology, Ruhr University Bochum, Bochum, Germany, ² Experimental Eye Research Institute, University Eye Hospital, Ruhr University Bochum, Bochum, Germany

Previous studies demonstrated that retinal damage correlates with a massive remodeling of extracellular matrix (ECM) molecules and reactive gliosis. However, the functional significance of the ECM in retinal neurodegeneration is still unknown. In the present study, we used an intraocular pressure (IOP) independent experimental autoimmune glaucoma (EAG) mouse model to examine the role of the ECM glycoprotein tenascin-C (Tnc). Wild type (WT ONA) and Tnc knockout (KO ONA) mice were immunized with an optic nerve antigen (ONA) homogenate and control groups (CO) obtained sodium chloride (WT CO, KO CO). IOP was measured weekly and electroretinographies were recorded at the end of the study. Ten weeks after immunization, we analyzed retinal ganglion cells (RGCs), glial cells, and the expression of different cytokines in retina and optic nerve tissue in all four groups. IOP and retinal function were comparable in all groups. Although RGC loss was less severe in KO ONA, WT as well as KO mice displayed a significant cell loss after immunization. Compared to KO ONA, less β III-tubulin⁺ axons, and downregulated oligodendrocyte markers were noted in WT ONA optic nerves. In retina and optic nerve, we found an enhanced GFAP⁺ staining area of astrocytes in immunized WT. A significantly higher number of retinal Iba1⁺ microglia was found in WT ONA, while a lower number of Iba1⁺ cells was observed in KO ONA. Furthermore, an increased expression of the glial markers *Gfap*, *Iba1*, *Nos2*, and *Cd68* was detected in retinal and optic nerve tissue of WT ONA, whereas comparable levels were observed in KO ONA. In addition, pro-inflammatory *Tnfa* expression was upregulated in WT ONA, but downregulated in KO ONA. Vice versa, a significantly increased anti-inflammatory

Tgfb1 expression was measured in KO ONA animals. We conclude that Tnc plays an important role in glial and inflammatory response during retinal neurodegeneration. Our results provide evidence that Tnc is involved in glaucomatous damage by regulating retinal glial activation and cytokine release. Thus, this transgenic EAG mouse model for the first time offers the possibility to investigate IOP-independent glaucomatous damage in direct relation to ECM remodeling.

Keywords: autoimmune glaucoma model, cytokines, microglia, optic nerve demyelination, reactive gliosis, tenascin-C

INTRODUCTION

Glaucomatous neurodegeneration is characterized by a progressive loss of retinal ganglion cells (RGCs) and their axons, which form the optic nerve. The molecular mechanisms of RGC degeneration are still not fully understood. In addition to increased intraocular pressure (IOP), immunological processes, glial activation, and remodeling of extracellular matrix (ECM) constituents are associated with glaucoma. In regard to the immune system, studies also indicate an alteration in serum antibodies against various retinal proteins in glaucoma patients with a normal IOP (1–3). The connection between an immune response and glaucoma disease with the characteristic loss of RGCs was already demonstrated in an experimental autoimmune glaucoma (EAG) rat model. Here, glaucomatous damage was induced by immunization with ocular proteins (4, 5). Furthermore, a pathological upregulation of specific ECM components could be demonstrated in this model (6). However, the relationship between a change in ECM components and glaucoma pathogenesis needs to be investigated.

The ECM consists of several molecules, including proteoglycans and glycoproteins and controls cellular key events such as adhesion, differentiation, migration, proliferation as well as survival (7–12). During development of the central nervous system (CNS), tenascin-C (Tnc) is strongly expressed by radial glial cells, immature astrocytes, and oligodendrocyte precursor cells (OPCs). It regulates axonal as well as neurite outgrowth and glial cells differentiation (11, 13–17). In this regard, axonal growth is modulated by specific Tnc isoforms, which contain a different combination of fibronectin type III domains (18). Moreover, Tnc expression is associated with the stem cell niche and regulates stem cell maintenance in addition to differentiation (19).

Abbreviations: Brn3a, brain-specific homeobox/POU domain protein 3a; CC1, coiled coil-1; Cd68, cluster of differentiation 68; EAG, experimental autoimmune glaucoma; ECM, extracellular matrix; ERG, electroretinogram; GCL, ganglion cell layer; GFAP, glial fibrillary acidic protein; Iba1, ionized calcium-binding adapter molecule 1; INL, inner nuclear layer; iNOS, inducible nitric oxide synthase; IOP, intraocular pressure; IPL, inner plexiform layer; KO, knockout; KO CO, control group tenascin-C knockout; KO ONA, immunized tenascin-C knockout; MBP, myelin basic protein; NFL, nerve fiber layer; Nos2, nitric oxide synthase 2; Olig2, oligodendrocyte transcription factor 2; ONA, optic nerve antigen; ONL, outer nuclear layer; OPC, oligodendrocytes precursor cell; OPL, outer plexiform layer; RGC, retinal ganglion cell; *Tgfb/TGF-β*, transforming growth factor-beta; Tnc, tenascin-C; TLR4, toll-like receptor 4; *Tnfa/TNF-α*, tumor necrosis factor-alpha; WT, wild type; WT CO, control group wild type; WT ONA, immunized wild type.

In the diseased brain, Tnc is highly re-expressed (11). For example, Tnc immunoreactivity is directly linked to amyloid-β plaques in Alzheimer's disease patients (20). A lack of Tnc leads to reduced deposits of amyloid-β plaques and protects from Alzheimer's disease (21). Furthermore, an immunomodulatory impact of Tnc was described by regulating the Th17 cell differentiation and activation (22, 23). Here, Tnc deficiency ameliorates experimental autoimmune encephalomyelitis in mice (24).

In the context of retinal neurodegenerative processes, Tnc also plays an important role (25). During retinal development, Tnc is found in the inner neuroblastic layer at embryonic day 13 (26). In the adult retina, Tnc is highly enriched in the outer and inner plexiform layers and is prominently expressed by amacrine and horizontal cells (27, 28). Additionally, optic nerve astrocytes synthesize Tnc (29, 30). ECM molecules can provide an inhibitory environment for neural regeneration and migration in the retina (30). A dramatic remodeling of ECM constituents was already described after ischemia and glaucomatous damage (25, 31). An upregulation of Tnc has been noted in a glaucoma animal model (32) as well as in open-angle glaucoma patients (33).

Tnc is a key regulator of the immune system and plays an important role during neuroinflammation and glial response (34–36). Moreover, expression of Tnc by astrocytes is regulated by cytokines secreted by microglia (37, 38). Microglia play an important role during neurodegenerative and neuroinflammatory processes (39). Their activation is characterized by an enhanced proliferation, migration, phagocytosis, and increased expression levels of neuroinflammatory molecules (40, 41). The neurotoxic M1-subtype has an amoeboid morphology and releases pro-inflammatory signaling molecules, like tumor necrosis factor-alpha (TNF-α) and inducible nitric oxide synthase (iNOS) (42–44). In contrast, the M2-phenotype is characterized by a morphology with ramified processes and the expression of anti-inflammatory cytokines, such as the transforming growth factor-beta (TGF-β) (45–47).

In this study, we used a Tnc deficient EAG mouse model to further analyze the importance of Tnc during retinal neurodegeneration and neuroinflammatory outcomes. We immunized wild type (WT) and Tnc knockout (KO) mice with an optic nerve antigen (ONA) homogenate and examined retinal and optic nerve damage as well as macro- and microglial activity. Furthermore, we determined the expression pattern of pro- and anti-inflammatory cytokines. The present study

was undertaken to address the role of Tnc in glaucomatous damage, retinal glial activation, myelination, and inflammatory cytokine release.

MATERIALS AND METHODS

Animals

Animals were housed under a 12 h light-dark cycle and had free access to chow and water. All procedures were approved by the animal care committee of North Rhine-Westphalia, Germany and performed according to the ARVO statement for the use of animals in ophthalmic and vision research. For the experiments, male and female littermates of 129/Sv WT and *Tnc* KO mice (48) were used at 6 weeks of age.

Immunization

WT (WT ONA) and KO (KO ONA) mice were immunized intraperitoneally with ONA (1 mg/ml) mixed with incomplete Freund's adjuvants (FA; 50 μ l) and 1 μ g pertussis toxin (PTx; both Sigma Aldrich, St. Louis, MO, USA) as described (49). To generate the ONA homogenate, fresh bovine eyes were obtained from a local slaughterhouse (Schlachthaus Wuppertal, Germany). As previously described, optic nerves were cut off behind the optic nerve head, cleaned from surrounding tissue and the dura mater was removed. Nerves were pulverized in a cooled mortar and then suspended in phosphate-buffered saline (PBS) (5). A final concentration of 1 mg/ml was set. FA acted

as an immunostimulatory and PTx was given to ensure the permeability of the blood retina barrier. Intraperitoneal PTx-application was repeated 2 days after immunization. Booster injections containing half of the initial dose were given intraperitoneally 4 and 8 weeks after initial immunization. The control groups (WT CO; KO CO) were injected with 1 ml sodium chloride (B. Braun Melsungen AG, Melsungen, Germany), FA and PTx. Ten weeks after immunization, retinae, and optic nerves were explanted for immunohistochemistry, quantitative real time PCR (RT-qPCR), and Western blot analyses. For RT-qPCR and Western blot, retinal as well as optic nerve tissue of both eyes from one animal were pooled.

Intraocular Pressure Measurements

Before IOP measurement, mice were anesthetized with a ketamine/xylazine mixture (120/16 mg/kg). Both eyes were analyzed and 10 readings of each eye were averaged. IOP measurements were performed before immunization in WT and KO mice at 5 weeks of age with a rebound tonometer (TonoLab; Icare; Oy; Finland; $n = 16$ /group) as previously described (50, 51). After immunization, IOP was measured weekly in all four groups until the end of the study ($n = 8$ /group).

Electroretinogram Recordings

Scotopic full-field flash electroretinograms (ERG) recordings (HMsERG system, OcuScience, Henderson, NV, USA) were taken 10 weeks after immunization in all groups ($n = 5$ /group).

TABLE 1 | List of primary and secondary antibodies to examine RGCs, macro-, and microglial cell types as well as Tnc in retinae and optic nerves via immunohistochemistry.

Primary antibody	Species, clonality/type	Dilution	Source (stock no.)/RRID	Secondary antibody	Species, type	Dilution/source
Brn-3a (flat-mount/retina)	Goat, polyclonal, IgG	1:300	Santa Cruz (Sc-31984) RRID:AB_2167511	Anti-goat Cy3	Donkey, IgG	1:250/Dianova
CC1 (optic nerve)	Mouse, monoclonal, IgG	1:100	Abcam (Ab16794) RRID:AB_443473	Anti-mouse Cy2	Goat, IgG	1:250/Dianova
GFAP (retina/optic nerve)	Mouse, monoclonal, IgG	1:300	Sigma-Aldrich (G3893) RRID:AB_477010	Anti-mouse Cy2	Goat, IgG	1:250/Dianova
Iba1 (flat-mount)	Rabbit, polyclonal, IgG	1:250	WAKO (019-19741) RRID:AB_839504	Anti-rabbit Cy2	Donkey, IgG	1:250/Dianova
MBP (optic nerve)	Rat, monoclonal, IgG	1:250	Bio-Rad (MCA409) RRID:AB_325004	Anti-rat Cy2	Goat, IgG	1:250/Dianova
Olig2 (optic nerve)	Rabbit, polyclonal, IgG	1:400	Merck (AB9610) RRID:AB_570666	Anti-rabbit Cy3	Goat, IgG	1:250/Dianova
Tnc (Kaf12) (retina)	Rabbit, polyclonal, IgG	1:250	(52)	Anti-rabbit Cy3	Goat, IgG	1:250/Dianova
β III-tubulin (optic nerve)	Mouse, monoclonal, IgG2b	1:300	Sigma-Aldrich (T 8660) RRID:AB_477590	Anti-mouse Cy2	Goat, IgG	1:250/Dianova

Primary and secondary antibodies, including species, clonality/type, dilution, and source/stock number were shown.

TABLE 2 | Adjustments for the ImageJ macro.

Protein	Tissue	Background subtraction	Lower threshold	Upper threshold
β III-tubulin	Optic nerve	50	29.45	82.18
GFAP	Retina	20	25.00	76.54
	Optic nerve	50	27.50	78.00
MBP	Optic nerve	50	7.62	62.45
Tnc	Retina	50	6.79	78.68

Data of background subtractions and upper/lower thresholds were present to determine the immunoreactive area [%].

as previously described (51). Mice were dark-adapted and anesthetized with a ketamine/xylazine mixture (120/16 mg/kg). Scotopic flash series with flash intensities at 0.1, 0.3, 1.0, 3.0, 10.0, and 25.0 cd/m² were recorded. Electrical potentials were analyzed with the ERGView 4.380R software (OcuScience) using a 150 Hz filter before evaluating a- and b-wave amplitudes.

Immunohistochemistry and Confocal Laser Scanning Microscopy

Eyes and optic nerves were dissected and fixed in paraformaldehyde (PFA) for 1 day, dehydrated in sucrose (30%) and embedded in Tissue-Tek freezing medium (Thermo Fisher Scientific, Cheshire, UK). Retinal cross-sections and optic nerve longitudinal sections (16 μ m) were cut with a cryostat (CM3050 S, Leica) and transferred onto Superfrost plus object slides (Menzel-Glaeser, Braunschweig, Germany). First, slices were blocked with 1% bovine serum albumin (BSA; Sigma-Aldrich), 3% goat serum (Dianova, Hamburg, Germany), and 0.5% TritonTM-X-100 (Sigma-Aldrich) in PBS for 1 hour (h) at room temperature (RT). Afterwards, the primary antibodies were diluted in blocking solution and incubated at RT overnight (Table 1). Sections were washed 3 times in PBS and incubated for 2 h with adequate secondary antibody (Dianova, Hamburg, Germany; Table 1) solution without TritonTM-X-100. Cell nuclei were detected with TO-PRO-3 (1:400; Thermo Fisher Scientific). The retinal and optic nerve slices were analyzed with a confocal laser-scanning microscope (LSM 510 META; Zeiss, Göttingen, Germany). Two sections per slide, 4 images per retina (400x magnification), and 3 images per optic nerve (200x magnification) were captured ($n = 4$ –5/group). In addition, a 630x magnification was used for colocalization staining in optic nerve sections with antibodies against CC1 (coiled-coil 1) and Olig2 (oligodendrocyte transcription factor 2). Accordingly, 4 images were taken per slide ($n = 5$ /group).

Laser lines and emission filters were adjusted using the Zeiss ZEN black software. Cropping of the images was done using Coral Paint Shop Pro X8 (Coral Corporation, Ottawa, Canada). Masked evaluation of the staining signal was performed with ImageJ software (ImageJ 1.51w, National Institutes of Health; Bethesda, MD, USA) as previously described (6, 53). Images were converted into gray scales and the background was subtracted. Then, the lower and upper threshold values were determined for each image (Table 2). The percentage of the area fraction was

measured using an ImageJ macro as previously described (53). This analysis was performed for immunohistochemical stainings against β III-tubulin, glial fibrillary acidic protein (GFAP), myelin basic protein (MBP), and Tnc. Cell countings were done for immunopositive Brn3a⁺ cells in retinal cross-sections and for Olig2⁺/CC1⁺ cells in optic nerve slices. Values were transferred to Statistica software and the WT CO group was set to 100% (V13.3; StatSoft (Europe), Hamburg, Germany).

Quantification of RGCs and Microglia in Retinal Flat-Mounts

Eyes were enucleated and fixed in 4% PFA at 4°C for 1 h. The retinae were dissected from the eye and prepared as flat-mounts ($n = 9$ /group). The tissue was fixed again in 4% PFA for 5 min and washed 3 times in PBS. Flat-mounts were blocked in 1% BSA, 3% donkey serum, and 2% TritonTM-X-100 in PBS at RT for 1 h. Next, incubation was performed with the RGC specific marker Brn3a [brain-specific homeobox/POU domain protein 3a; (54, 55)] and microglia marker Iba1 [ionized calcium-binding adapter molecule 1; (56)] for 2 days at 4°C. Following PBS washing (3 \times 20 min), flat-mounts were incubated with secondary antibodies donkey anti-goat Cy3, donkey anti-rabbit Alexa Fluor 488, and TO-PRO-3 (1:400) in blocking solution without TritonTM-X-100 at RT for 2 h. Microscopic images were captured using Axio Zoom.V16 (Zeiss, Göttingen, Germany). Flat-mounts were divided into 16 quadrants (200 \times 200 μ m) and Brn3a⁺ and Iba1⁺ cells were counted. Groups were compared using two-way ANOVA followed by Tukey's *post-hoc* test. The WT CO group was set to 100%.

Western Blotting

Retinal tissue ($n = 5$ /group) was homogenized in 150 μ l and optic nerve tissue ($n = 5$ /group) in 100 μ l lysis buffer (60 mM n-octyl- β -D-glucopyranoside, 50 mM sodium acetate, 50 mM Tris chloride, pH 8.0 and 2 M urea) containing a protease inhibitor cocktail (Sigma-Aldrich) on ice for 1 h. Prior to lysis, the optic nerve tissue was incubated in liquid nitrogen. Subsequently, all samples were centrifuged at 14,000 \times g at 4°C for 30 min and the supernatant was applied to determine the protein concentration. A BCA Protein Assay kit (Pierce, Thermo Fisher Scientific, Rockford, IL, USA) was used for retinal tissue. For optic nerves, the Qubit[®] Protein Assay kit (Life Technologies GmbH, Darmstadt, Germany) was used according to manufacturer's instructions. 4x SDS buffer was added to each protein sample (20 μ g) and denatured at 94°C for 5 min. After separation via SDS-PAGE (10% gels, respectively, 4–12% polyacrylamide gradient gels), proteins were transferred to a polyvinylidene difluoride (PVDF) membrane (Roth, Karlsruhe, Germany) by Western blotting (1–2 h and 75 mA). Membranes were blocked (5% w/v milk powder in TRIS-buffered saline (TBS) with 0.05% Tween[®] 20; TBST) at RT for 1 h and incubated with the primary antibody (Table 3) in blocking solution at 4°C overnight. On the next day, membranes were washed with TBST and incubated with horseradish peroxidase (HRP) coupled secondary antibodies (Table 3) in blocking solution at RT for 2 h. Excess antibody was washed off with TBST. ECL Substrate (Bio-Rad Laboratories GmbH, München,

TABLE 3 | List of primary and secondary antibodies for western blotting.

Primary antibody	Species, clonality, type	Dilution	Source (stock no.)/RRID	Secondary antibody, species, type	Dilution	Source	kDa
Actin	Mouse, monoclonal, IgG	1:5,000	BD Bioscience (612657) RRID:AB_399901	Anti-mouse, IgG + IgM HRP	1:5,000	Dianova	42
GFAP	Rabbit, polyclonal, IgG	1:10,000	Dako (Z0334) RRID:AB_10013382	Anti-rabbit, IgG HRP	1:10,000	Dianova	50
MBP	Rat, monoclonal, IgG	1:1,000	Bio-Rad (MCA409) RRID:AB_325004	Anti-rat, IgG HRP	1:5,000	Dianova	20
Olig2	Rabbit, polyclonal, IgG	1:500	Merck (AB9610) RRID:AB_570666	Anti-rabbit, IgG HRP	1:5,000	Dianova	32 and 50
Tnc (Kaf12)	Rabbit, polyclonal, IgG	1:5,000	(52)	Anti-rabbit, IgG HRP	1:5,000	Dianova	~ 250 and > 250
Vinculin	Mouse, monoclonal, IgG1	1:200	Sigma-Aldrich (V 9131) RRID:AB_477629	Anti-mouse, IgG + IgM HRP	1:5,000	Dianova	116

Primary and secondary antibodies, including species, clonality, type, dilution, source, and stock number are listed. Relative quantification of band intensity was done against the housekeeping proteins actin or vinculin. HRP, horseradish peroxidase; kDa, Kilodalton.

Germany) was applied to develop the membrane (mixed 1:1 for 5 min). Finally, protein immunoreactivity was detected with a MicroChemi Chemiluminescence Reader (Biostep, Burkhardtendorf, Germany). Band intensity was analyzed using ImageJ software and normalized to a corresponding reference protein (actin/vinculin). The normalized values of the Western blot results were given in arbitrary units (a.u.).

RNA Isolation, cDNA Synthesis, and RT-qPCR

Retinal tissue was homogenized by trituration using a pipette ($n = 5/\text{group}$). The RNA isolation of the retina was carried out according to the manufacturer's introduction using the Gene Elute Mammalian Total RNA Miniprep Kit (Sigma-Aldrich, St. Louis, MO, USA). For total RNA isolation of optic nerve tissue, the ReliaPrep™ RNA Tissue Miniprep System (Promega, Madison, WI, USA) was taken. Prior to isolation, optic nerve tissue was incubated in liquid nitrogen and then homogenized with a pestle ($n = 5/\text{group}$). An additional DNase digestion at RT for 15 min ensured that no genomic DNA contaminated RNA was obtained. The concentration and purity of the isolated RNA was determined photometrically using the BioSpectrometer® (Eppendorf, Hamburg, Germany). One microgram RNA and random hexamer primers were applied for reverse transcription using a cDNA synthesis kit (Thermo Fisher Scientific, Waltham, MA, USA). RT-qPCR experiments were done with SYBR Green I in a Light Cycler 96® (Roche Applied Science, Mannheim, Germany). For each primer pair (Table 4), efficiencies were determined by a dilution series of 5, 25, and 125 ng cDNA. Expression in retina and optic nerve tissue was normalized against the housekeeping genes β -actin (*Actb*) and 18S ribosomal RNA (*Rn18S*), respectively.

Statistical Analysis

Immunohistological, Western blot, IOP, and ERG data of control WT (WT CO) and KO (KO CO) as well as ONA-immunized WT (WT ONA) and KO (KO ONA) were analyzed by two-way ANOVA followed by Tukey's *post-hoc* test using Statistica software (V13.3; StatSoft (Europe), Hamburg, Germany). Results of IOP measurements were presented as mean \pm standard error mean (SEM) \pm standard deviation (SD). ERG recordings, immunohistochemical, and Western blot data were shown as mean \pm SEM. Analyses of Tnc protein levels in WT mice via immunohistochemistry and Western blot were analyzed via Student *t*-test and presented as mean \pm SEM. For RT-qPCR results, groups were compared using the pairwise fixed reallocation and randomization test (REST® software) and were presented as median \pm quartile \pm minimum/maximum (57).

RESULTS

No Changes in IOP and Retinal Functionality in the EAG Mouse Model

IOP measurements were performed before immunization in 5-week-old WT (WT CO) and KO (KO CO; Figure 1A). After immunization, IOP was measured weekly in control and immunized WT (WT ONA) and KO (KO ONA) animals until the end of the study. At 5 weeks of age (-1), we observed no significant differences in the IOP of WT CO (9.8 ± 0.2 mmHg) and KO CO (9.7 ± 0.1 mmHg; $p = 1.0$). Furthermore, no changes in the IOP were found in control and immunized groups throughout the study (Supplementary Table 1).

To determine possible retinal function deficits, induced by ONA-immunization, we performed ERG recordings of control and immunized WT and KO mice. Under scotopic

TABLE 4 | List of primer pairs used for mRNA analyses by RT-qPCR.

Gene	Primer sequence	Amplicon size (bp)	Primer efficiency, retina/optic nerve	GenBank accession number
<i>Rn18S_for</i>	GCAATTATCC CCATGAACG	68	-/1	NR_003278.3
<i>Rn18S_rev</i>	GGGACTTAAT CAACGCAAGC			
<i>Actb_for</i>	CTAAGGCCAA CCGTGAAAAG	104	0.84/-	NM_007393.3
<i>Actb_rev</i>	ACCAGAGGCAT ACAGGGACA			
<i>Cd68_for</i>	GGACCCACAAC TGCTACTCA	60	0.89/1	NM_001291058.1
<i>Cd68_rev</i>	AATTGTGGCAT TCCCATGAC			
<i>Gfap_for</i>	ACAGACTTTCTC CAACCTCCAG	63	0.84/1	NM_001131020
<i>Gfap_rev</i>	CCTTCTGACAC GGATTTGGT			
<i>Iba1_for</i>	GGATTTGCAG GGAGGAAAAG	92	0.80/0.91	NM_019467.3
<i>Iba1_rev</i>	TGGGATCATC GAGGAATTG			
<i>Nos2_for</i>	CTTTGCCAC GGACGAGAC	66	1/0.70	NM_010927.3
<i>Nos2_rev</i>	TCATTGTACTCT GAGGGCTGAC			
<i>Tgfb1_for</i>	TGGAGCAACA TGTGGAAGCTC	73	1/0.91	NM_011577.2
<i>Tgfb1_rev</i>	GTCAGCAGC CGGTTACCA			
<i>Tnfa_for</i>	TCTTCTCATTCC TGCTTGTGG	101	1/0.97	NM_013693.3/ NM_001278601.1
<i>Tnfa_rev</i>	GAGGCCATTTG GGAAGTTCT			

For evaluation of mRNA-levels, *Actb*, and *Rn18S* served as housekeeping genes. Primer sequence, predicted amplicon size, primer efficiency for retinae and optic nerves and GenBank accession number are listed. Bp, base pairs; for, forward; rev, reverse.

conditions, a-wave responses arise from rod-photoreceptors, while b-waves represent the rod bipolar and Müllerglia cell response. In all four conditions no significant differences were observed between control and immunized WT and KO animals (Figures 1B,C; Supplementary Table 2). Therefore, we concluded that photoreceptor and bipolar cell function was not affected in this EAG mouse model.

Significant RGC Loss Following Immunization

Previous studies of an EAG rat model showed a significant reduction of RGC numbers 4 weeks post immunization with ONA (4, 58). Additionally, an upregulation of *Tnc* was found before significant RGC loss occurred (6). In our EAG mouse model, we detected unaltered *Tnc* protein levels 10 weeks after immunization

(Supplementary Table 3, Supplementary Figure 1). Based on these findings, immunohistochemical stainings of RGCs were performed with an antibody against *Brn3a*, which specifically detects RGCs (Figure 2, Supplementary Table 4). The evaluation of RGCs in retinal cross-sections showed a significant reduction in the percentage of *Brn3a*⁺ cells in WT ONA compared to WT CO as well as to KO CO (WT ONA: 73.1 ± 6.1% *Brn3a*⁺ cells vs. WT CO: 100.0 ± 4.2% *Brn3a*⁺ cells; *p* = 0.004 and KO CO: 92.2 ± 3.9% *Brn3a*⁺ cells, *p* = 0.04, Figures 2A,B). Interestingly, no significant differences were detected between control and immunized KO in horizontal cross-sections (KO CO: 92.2 ± 3.9% *Brn3a*⁺ cells vs. KO ONA: 83.7 ± 8.7% *Brn3a*⁺ cells, *p* = 0.57, Figures 2A,B).

To further characterize the RGC population, we counted *Brn3a*⁺ cells in retinal flat-mounts (Figure 2C). We determined the total amount (Figure 2D) as well as the number of *Brn3a*⁺ cells within the central (Figure 2E) and peripheral (Figure 2F) area of the retina. A significant reduction in the total number was observed in immunized WT compared to both control genotypes (WT ONA: 80.3 ± 1.5% *Brn3a*⁺ cells vs. WT CO: 100.0 ± 2.0% *Brn3a*⁺ cells, *p* < 0.001, KO CO: 98.2 ± 3.3% *Brn3a*⁺ cells, *p* < 0.001). Also, a significant loss of RGCs was detected in KO ONA mice (86.9 ± 3.1% *Brn3a*⁺ cells) compared to KO CO (*p* = 0.02) and WT CO (*p* = 0.01). A comparable percentage of *Brn3a*⁺ cells was also observed in the central retina. So, immunized WT and KO animals showed a significant decline of RGCs compared to the corresponding control groups (WT ONA: 82.7 ± 1.7% *Brn3a*⁺ cells vs. WT CO: 100.0 ± 2.5% *Brn3a*⁺ cells, *p* < 0.001 and KO ONA: 86.3 ± 3.7% *Brn3a*⁺ cells vs. KO CO: 97.8 ± 2.9% *Brn3a*⁺ cells, *p* = 0.03). No significant differences were found between both immunized genotypes (*p* = 0.80). Furthermore, a decrease in the RGC density was verified in the peripheral area. Retinae of the WT ONA group (77.0 ± 1.8% *Brn3a*⁺ cells) displayed a loss of about 25% RGCs compared to WT CO (100.0 ± 1.7% *Brn3a*⁺ cells, *p* < 0.001). A significant reduction was also found in the comparison of KO CO and KO ONA (KO CO: 99.0 ± 4.1% *Brn3a*⁺ cells vs. KO ONA: 87.1 ± 2.8% *Brn3a*⁺ cells, *p* = 0.02). However, KO ONA showed a decrease of about 15% in the peripheral part compared to WT CO group (*p* = 0.01).

Although not statistically significant, we found a trend to a weaker RGC damage in immunized KO compared to WT ONA.

Optic Nerve Degeneration Post ONA-Immunization in WT Mice

To analyze a possible degeneration of RGC axons, immunoreactivity of β III-tubulin was examined in optic nerve longitudinal sections of control and immunized WT and KO animals (Figure 3A). The immunopositive β III-tubulin area was significantly reduced in immunized WT (30.85 ± 8.55% β III-tubulin⁺ area) compared to WT CO (100.00 ± 18.35% β III-tubulin⁺ area, *p* = 0.04, Figure 3B). Also, the β III-tubulin⁺ area was decreased in WT ONA compared to both KO conditions (KO CO: 93.66 ± 19.18% β III-tubulin⁺ area, *p* = 0.06 and KO ONA: 119.93 ± 13.48% β III-tubulin⁺ area, *p* < 0.01).

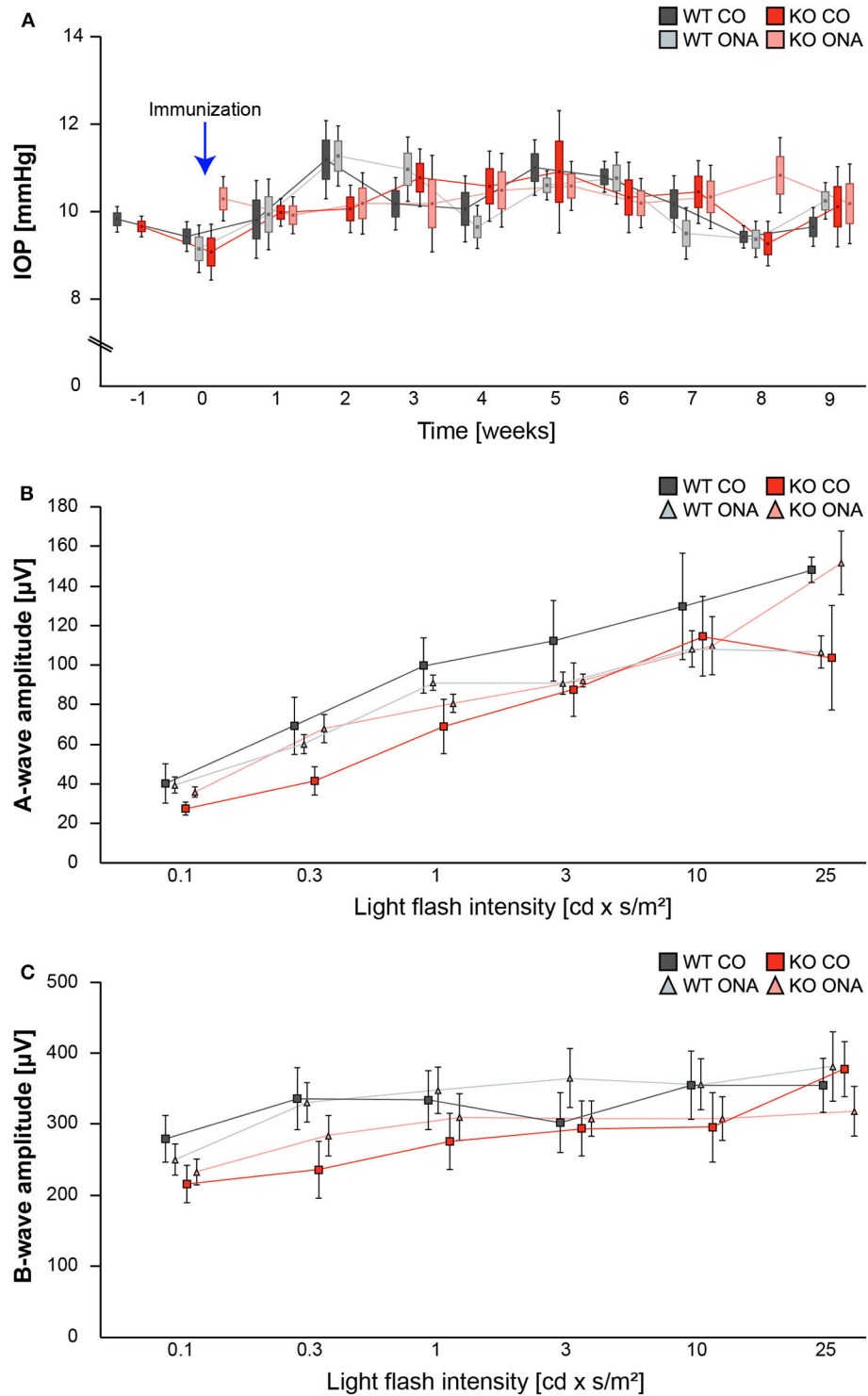
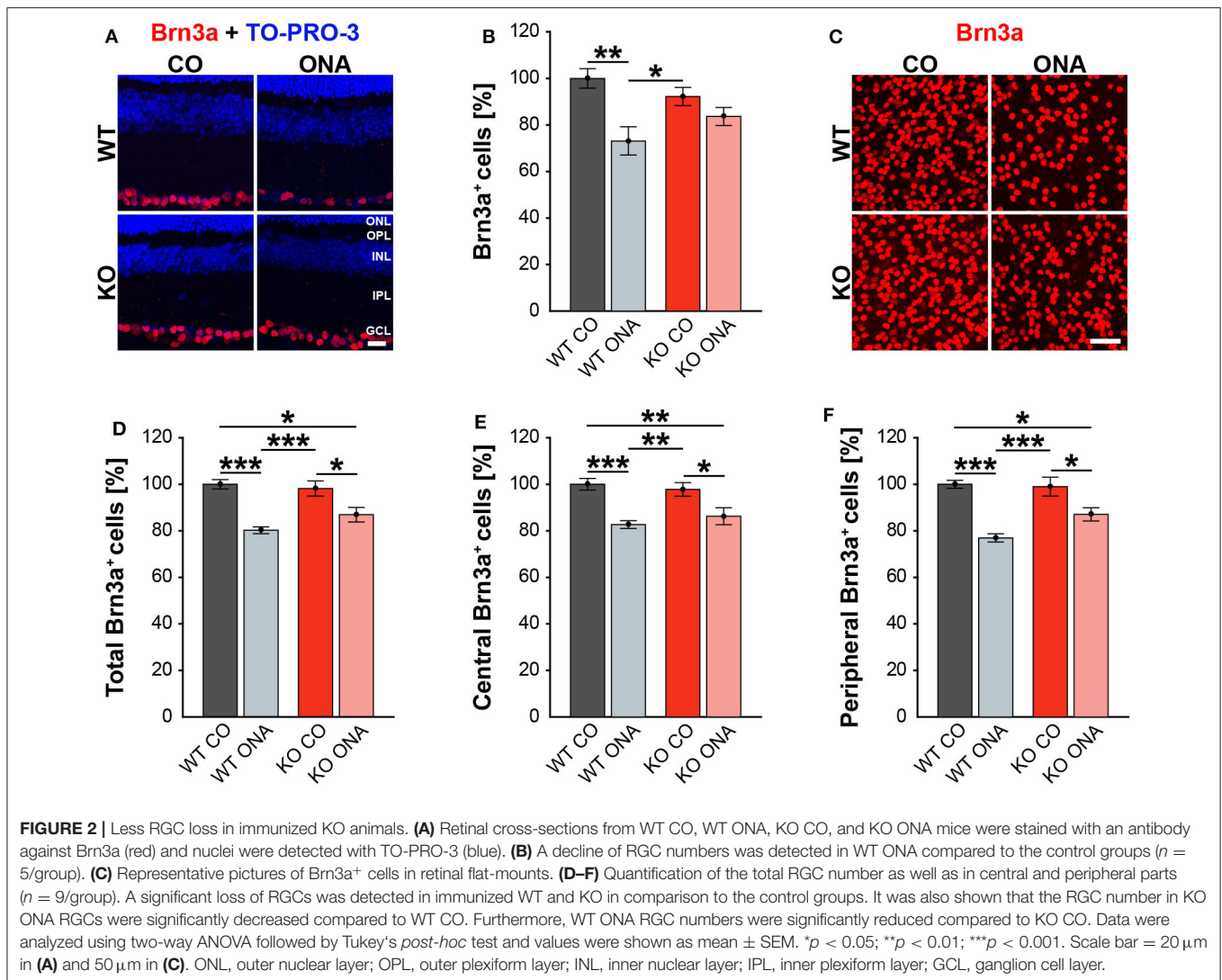


FIGURE 1 | IOP and ERG recordings were not altered after immunization of WT and KO mice. **(A)** IOP measurements were performed before immunization in 5 weeks old WT and KO mice (−1; $n = 16/\text{group}$). Then, IOP was determined weekly in immunized and control WT and KO until the end of the study ($n = 8/\text{group}$). No significant changes could be detected between all groups. **(B,C)** ERG recordings 10 weeks after initial immunization in control and immunized WT and KO mice. No changes in a-wave **(B)** and b-wave **(C)** amplitudes could be detected in control and immunized WT and KO mice ($n = 5/\text{group}$). Data were analyzed using two-way ANOVA followed by Tukey's *post-hoc* test and present as mean \pm SEM \pm SD in **(A)** and mean \pm SEM in **(B,C)**. cd, candela; IOP, intraocular pressure; μV , micro volt; m, minutes; s, seconds.



Extenuated Macroglial Reactivity After Immunization in KO Mice

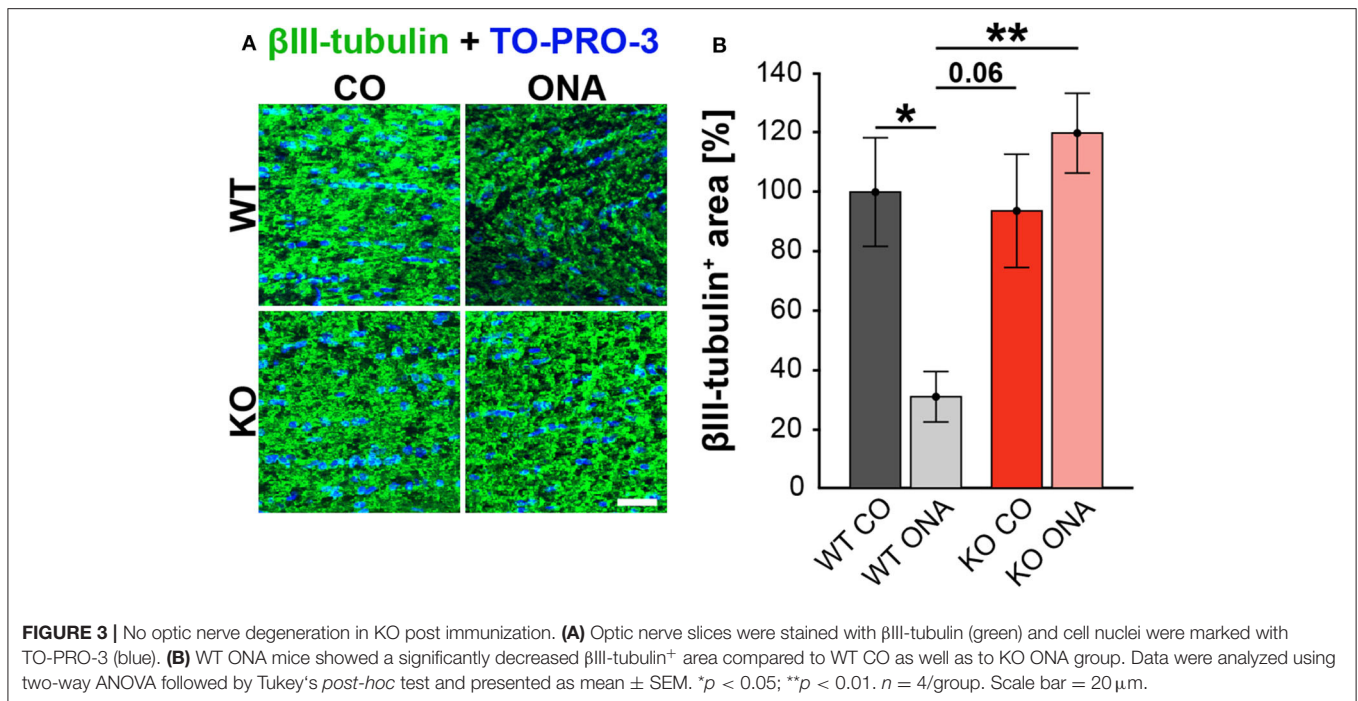
Our results showed a decrease in the RGC number 10 weeks after immunization in WT and KO animals. Next, we investigated, if this glaucomatous neurodegeneration is associated with an altered macroglial response. Therefore, we analyzed the immunoreactivity of GFAP⁺ astrocytes in retinal cross-sections. GFAP stained astrocytes were mainly localized in the ganglion cell layer (GCL; **Figure 4A**). The GFAP⁺ area was increased in WT ONA ($167.22 \pm 18.61\%$ GFAP⁺ area) compared to the control groups (WT CO: $100.00 \pm 9.28\%$ GFAP⁺ area, $p = 0.01$ and KO CO: $105.81 \pm 4.54\%$ GFAP⁺ area, $p = 0.02$, **Figure 4B**). Interestingly, no changes in the GFAP signal area were found in KO ONA ($142.49 \pm 8.19\%$ GFAP⁺ area) compared to KO CO ($p = 0.18$) as well as to WT CO ($p = 0.11$). The statistical comparison of both immunized genotypes showed no significant differences ($p = 0.46$).

Then, we evaluated GFAP protein levels via Western blot. For GFAP, a prominent band was detected at 50 kDa (**Figure 4C**).

Relative quantification verified a slight, but not statistically significant, increase in the GFAP protein concentration in WT after immunization (WT ONA: 1.15 ± 0.25 a.u. vs. WT CO: 0.76 ± 0.11 a.u., $p = 0.73$ and KO CO: 0.91 ± 0.40 a.u., $p = 0.92$, **Figure 4D**). No changes were observed in the GFAP level of control and immunized KO animals (KO ONA: 0.98 ± 0.23 a.u., $p = 0.99$).

We also analyzed the mRNA expression of *Gfap* in retinae via RT-qPCR (**Figures 4E–G, Supplementary Table 5**). Analysis revealed comparable levels of *Gfap* in KO CO and WT CO (1.4-fold, $p = 0.11$, **Figure 4E**). A significant increase of *Gfap* mRNA expression levels was observed in WT ONA (WT CO vs. WT ONA: 1.7-fold, $p = 0.04$, **Figure 4F**), whereas no differences could be detected in KO ONA (KO CO vs. KO ONA: 1.2-fold, $p = 0.40$, **Figure 4F**). The expression was comparable in both immunized genotypes (1.0-fold, $p = 0.99$, **Figure 4G**).

For GFAP, a thread-like staining pattern was observed in optic nerve slices (**Figure 5A**). The evaluation of the GFAP immunoreactivity in optic nerve sections also showed no



increased macroglial area in KO post immunization (KO ONA: $134.30 \pm 23.57\%$ GFAP⁺ area vs. KO CO: $147.18 \pm 31.27\%$ GFAP⁺ area, $p = 0.98$ and WT CO: $100.00 \pm 17.72\%$ GFAP⁺ area, $p = 0.70$, **Figure 5B**). Moreover, a nearly doubled GFAP intensity was observed in WT ONA ($196.70 \pm 13.60\%$ GFAP⁺ area) compared to the corresponding control group ($p = 0.04$).

Furthermore, protein levels of GFAP via Western blot analyses were comparable between all four groups (**Figure 5C**). However, the band intensity in WT ONA group was tentatively increased compared to the control group (WT ONA: 1.36 ± 0.29 a.u. vs. WT CO: 1.02 ± 0.27 a.u., $p = 0.68$, **Figure 5D**). Equal protein levels were found between control and KO ONA animals (KO CO: 0.82 ± 0.11 a.u. vs. KO ONA: 0.84 ± 0.10 a.u., $p = 0.99$).

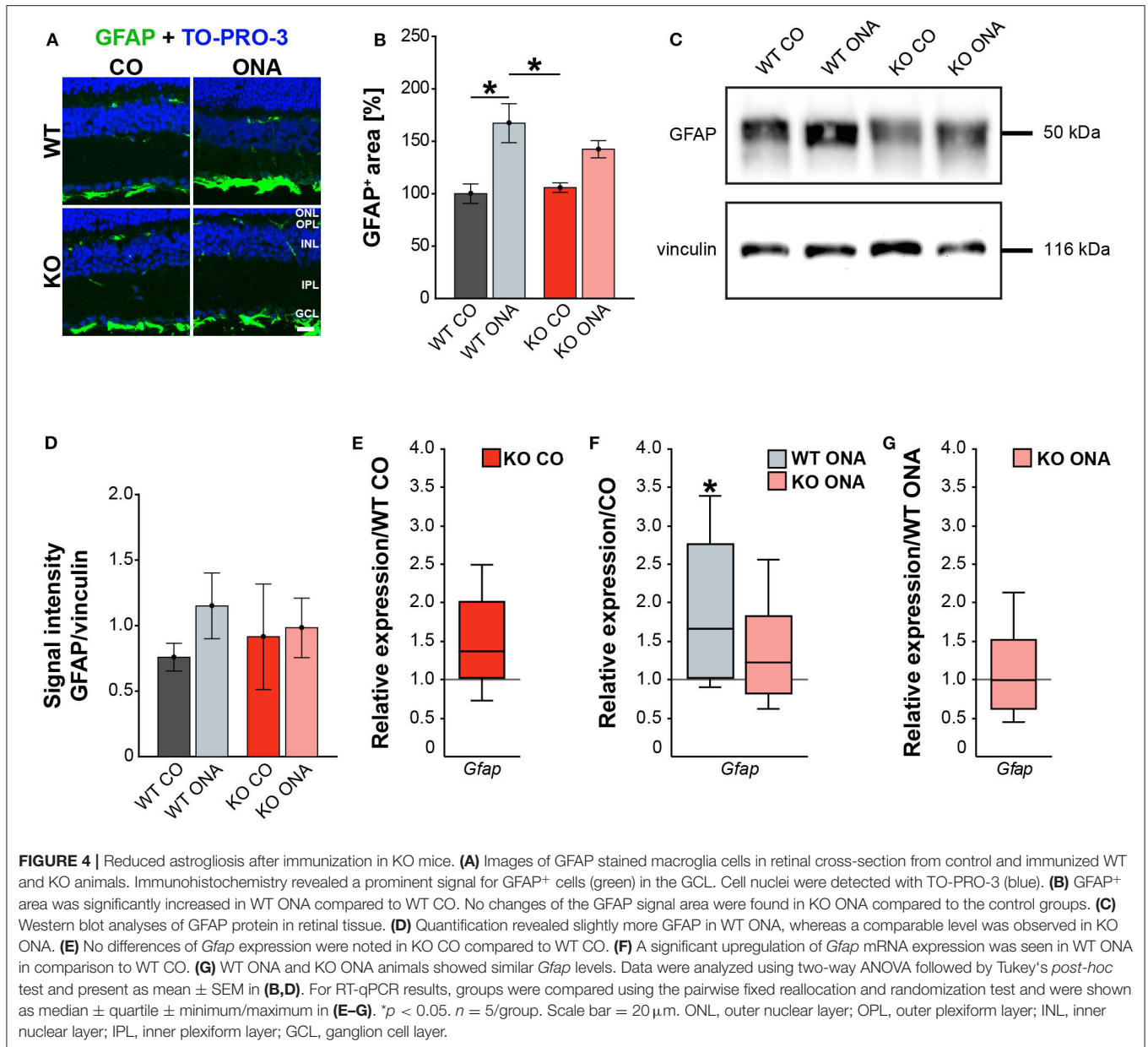
Finally, the RT-qPCR results of the optic nerve tissue showed no changes in *Gfap* expression between both control groups (WT CO vs. KO CO: 1.1-fold, $p = 0.54$, **Figure 5E**, **Supplementary Table 5**). In line with the immunohistochemical results, we found a slightly enhanced mRNA level in WT ONA (WT CO vs. WT ONA: 1.4-fold, $p = 0.07$, **Figure 5F**), whereas the KO ONA animals exhibited a reduction of *Gfap* expression (KO CO vs. KO ONA: 0.5-fold, $p < 0.05$). Interestingly, in a direct comparison of the two immunized groups, *Gfap* expression was significantly reduced in KO animals (WT ONA vs. KO ONA: 0.4-fold, $p = 0.02$, **Figure 5G**).

In summary, we concluded that *Tnc* deficiency resulted in a diminished macroglial reaction during retinal and optic nerve degeneration in the EAG mouse model.

Decreased Demyelination After ONA-Immunization in KO Mice

Our study demonstrates RGC degeneration in WT and KO animals after immunization. Furthermore, we noted

that *Tnc* deficiency resulted in a diminished macroglial response. Finally, we analyzed the impact of ONA-immunization on oligodendroglia in optic nerve tissue. The oligodendrocytes appear in two different populations, as immature OPCs and as myelinating, mature oligodendrocytes. To analyze both oligodendrocyte populations separately, an immunohistochemical colocalization staining was performed using the markers Olig2 and CC1. Olig2 is expressed by oligodendrocytes of all stages (59). In contrast, CC1 is only expressed by mature oligodendrocytes (60). Colocalization identified double positive cells as mature and single Olig2⁺ cells as immature oligodendrocytes. Immunohistochemical stainings revealed fewer Olig2⁺ cells in the WT ONA group compared to the other groups. Interestingly, there were more Olig2⁺ cells in KO ONA than in WT ONA (**Figure 6A**). $76.3 \pm 1.6\%$ Olig2⁺ cells were found in WT ONA, which indicates a significant oligodendrocyte loss over 25% compared to control WT ($100.0 \pm 3.5\%$ Olig2⁺ cells, $p < 0.001$, **Figure 6B**). The number of Olig2⁺ cells was also significantly decreased in WT ONA compared to KO CO ($p = 0.04$). No differences were observed between both *Tnc* deficient groups (KO CO: $90.2 \pm 2.4\%$ Olig2⁺ cells vs. KO ONA: $95.2 \pm 4.9\%$ Olig2⁺ cells, $p = 0.71$). Most interestingly, we verified significant differences between both immunized groups ($p < 0.01$). The number of double-positive (Olig2⁺/CC1⁺) mature oligodendrocytes was clearly reduced in WT ONA compared to all other groups (**Figure 6A**). The statistical evaluation demonstrated only $64.7 \pm 5.8\%$ Olig2⁺/CC1⁺ cells in WT ONA, whereas KO ONA exhibited $107.8 \pm 8.9\%$ Olig2⁺/CC1⁺ cells in optic nerve slices ($p = 0.002$, **Figure 6C**). Also, immunized WT showed a significant loss of mature oligodendrocytes compared to WT CO ($100.0 \pm 8.3\%$ Olig2⁺/CC1⁺ cells,



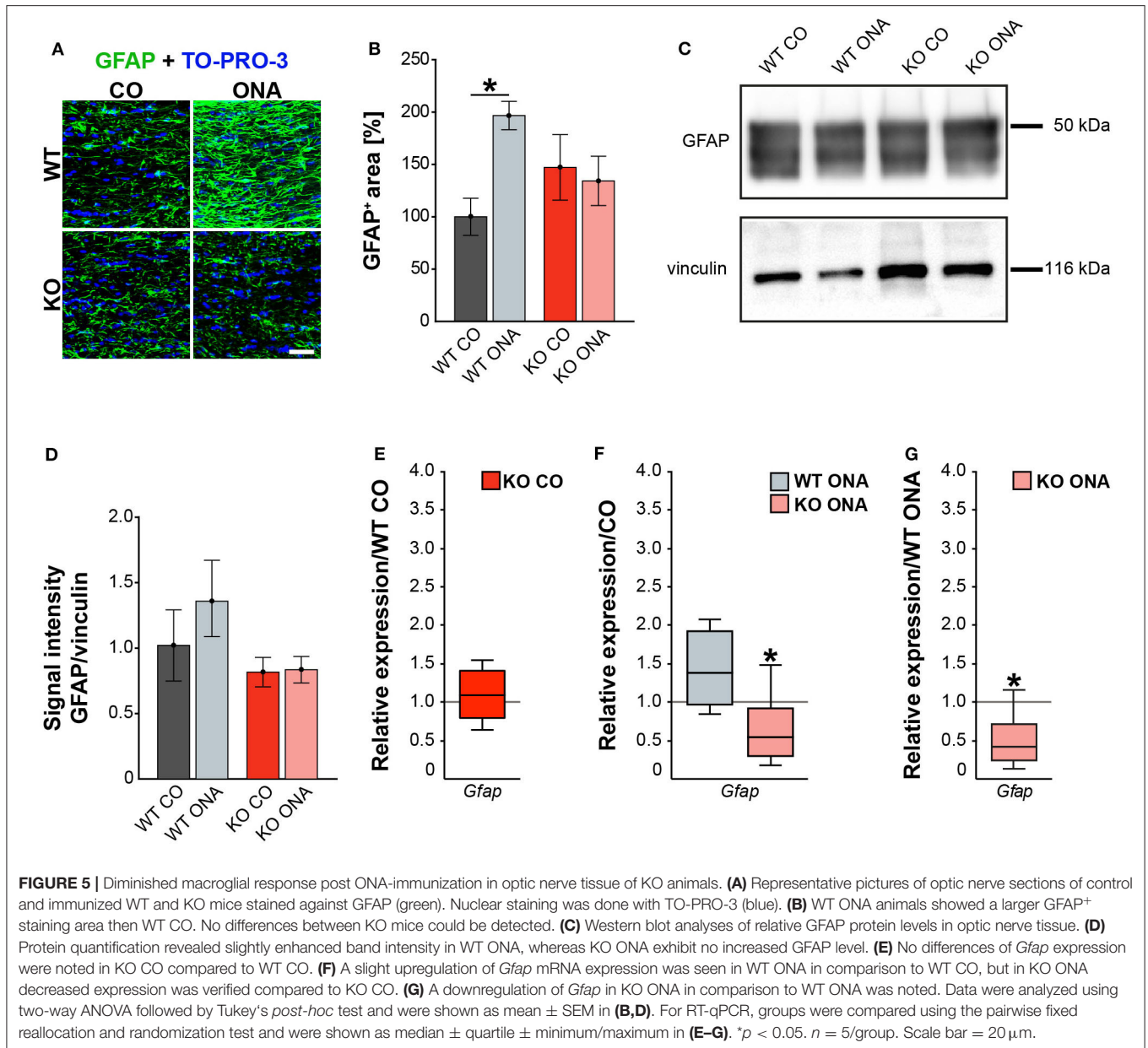
$p = 0.01$) and KO CO ($118.4 \pm 3.5\%$ Olig2⁺/CC1⁺ cells, $p < 0.001$).

To consolidate the immunohistochemistry results, we analyzed the Olig2 protein level in optic nerves by Western blot analyses (**Figure 6D**). For Olig2, we observed two bands at 32 and 50 kDa. A slight but not significantly decrease of the band intensity was found in WT ONA (0.36 ± 0.10 a.u.) compared to the corresponding control group (0.86 ± 0.41 a.u., $p = 0.41$, **Figure 6E**). Equal Olig2 protein levels were observed in KO CO (0.62 ± 0.10 a.u.) and KO ONA (0.67 ± 0.12 a.u., $p = 0.99$). Missing of *Tnc* resulted in an equal Olig2 protein level in both immunized groups ($p = 0.76$).

Finally, we also investigated MBP on protein level via immunohistochemistry and Western blot. This protein is

specifically expressed by myelinating oligodendrocytes (61). Immunohistochemical staining revealed significantly reduced MBP immunoreactivity in WT ONA (**Figure 7A**). Statistical analyses discovered a decreased MBP signal in WT ONA ($46.22 \pm 11.30\%$ MBP⁺ area) compared to WT CO ($100.00 \pm 7.47\%$ MBP⁺ area, $p = 0.001$), KO CO ($88.76 \pm 4.93\%$ MBP⁺ area, $p = 0.01$) and KO ONA ($109.79 \pm 7.01\%$ MBP⁺ area, $p < 0.001$, **Figure 7B**).

MBP was examined on protein level via Western blot analyses and a prominent protein band was detected at 20 kDa (**Figure 7C**). Quantitative analyses revealed comparable MBP protein levels in control (WT CO: 0.76 ± 0.07 a.u., KO CO: 0.56 ± 0.09 a.u.) and ONA mice (WT ONA: 0.52 ± 0.09 a.u., KO ONA: 0.51 ± 0.1 a.u., **Figure 7D**).

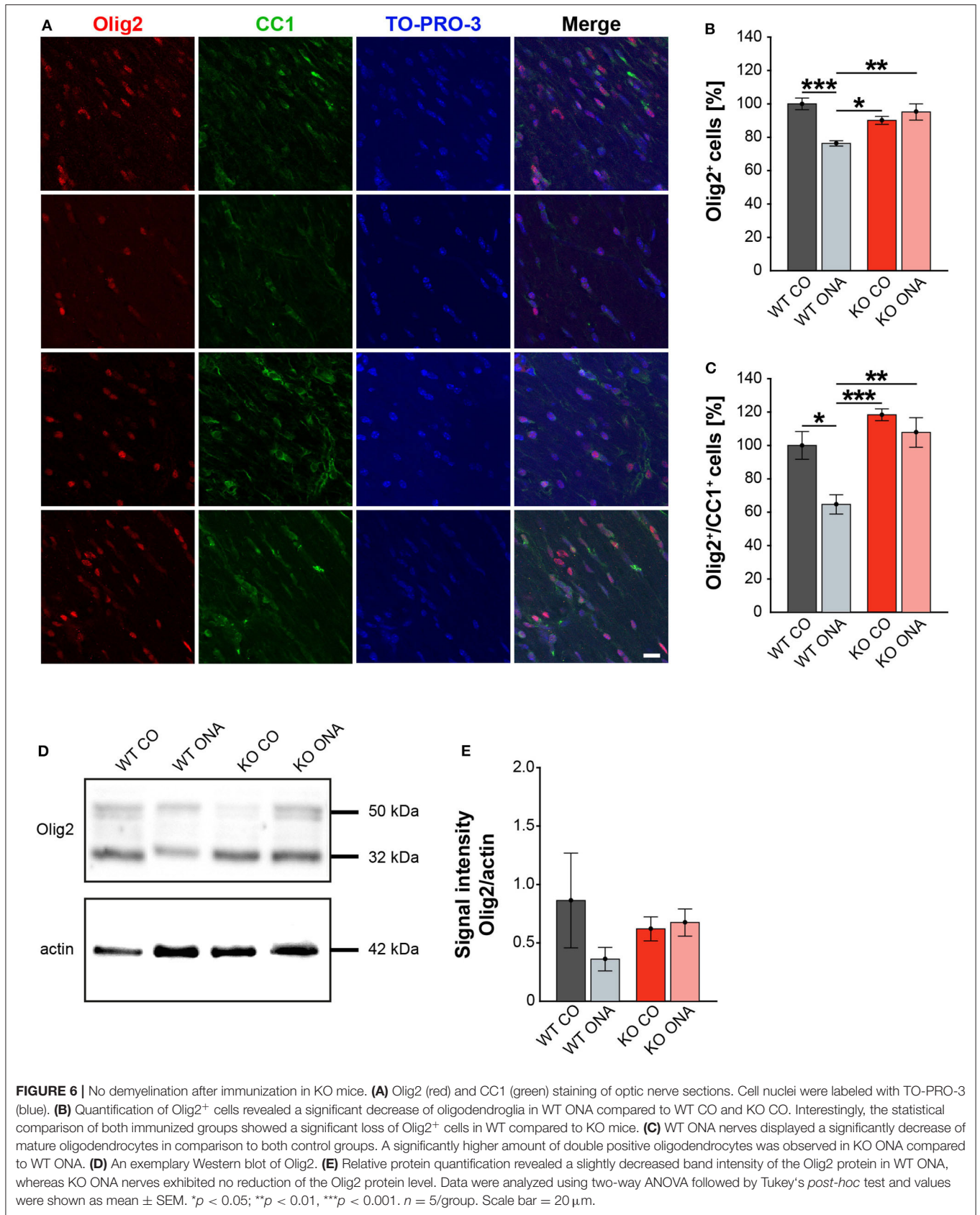


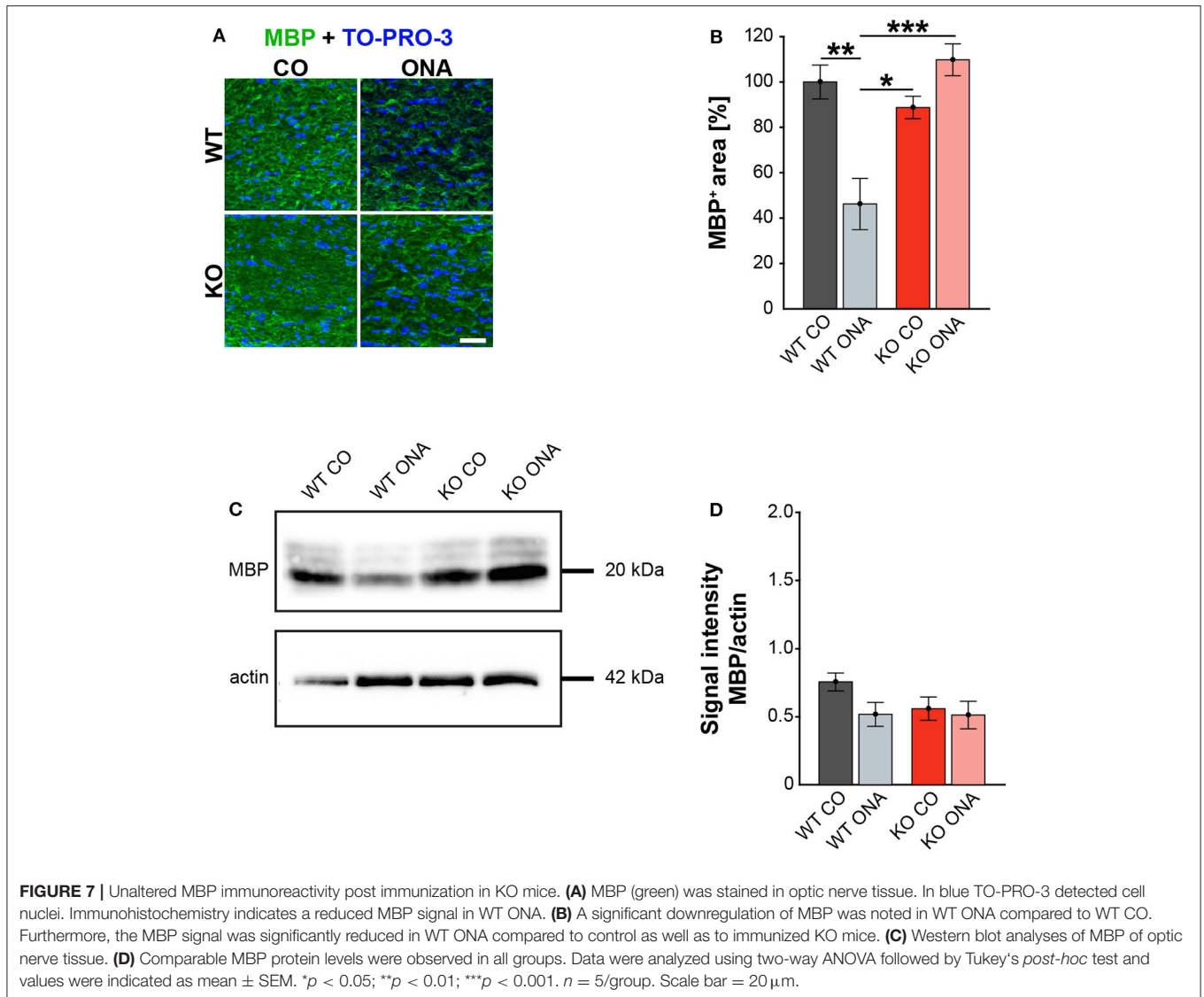
In conclusion, we found a significant decrease in mature as well as immature oligodendroglia in WT after immunization. Remarkably, immunized *Tnc* deficient mice showed no demyelination.

Decreased Number of Microglia and Declined Microglial Response in KO ONA Mice

Neurodegeneration is often accompanied by reactive microgliosis. In order to analyze the microglia population in the EAG mouse model and the effects of immunization, we performed immunohistochemical staining of retinal flat-mounts using an Iba1 antibody (Figure 8A, Supplementary Table 4). The number of Iba1⁺ cells in the total as well as in the central

and peripheral area of the retina was evaluated (Figures 8B–D). A significant increase in microglia numbers was detected in WT ONA ($123.0 \pm 2.4\%$ Iba1⁺ cells) compared to control WT and KO in the total retina (WT CO: $100.0 \pm 2.9\%$ Iba1⁺ cells, $p < 0.001$ and vs. KO CO: $102.3 \pm 5.7\%$ Iba1⁺ cells; $p = 0.002$, Figure 8B). No differences were found between both control groups ($p = 0.97$). Remarkably, a significantly lower number of Iba1⁺ cells was observed after immunization in KO ONA (KO ONA: $84.5 \pm 2.7\%$ Iba1⁺ cells) compared to WT ONA ($p < 0.001$), WT CO ($p = 0.03$), and KO CO ($p < 0.01$). Also, in the central part of the retina 20% more Iba1⁺ cells were detected in WT ONA ($122.5 \pm 2.9\%$ Iba1⁺ cells) compared to the corresponding control group (WT CO: $100.0 \pm 3.5\%$ Iba1⁺ cells, $p < 0.01$, Figure 8C). Immunized WT





also showed significantly more microglial cells compared to control ($p < 0.001$) and immunized KO mice ($p < 0.001$). In KO CO, we counted $98.1 \pm 5.8\%$ Iba1⁺ cells, whereas KO ONA only has $84.0 \pm 2.9\%$ Iba1⁺ cells ($p = 0.08$). A reduced microglia number was noted in KO ONA compared to WT CO ($p = 0.04$). Equal numbers of microglial cells were seen in both control groups ($p = 0.99$). Similarly, the number of microglia in WT ONA ($123.6 \pm 3.4\%$ Iba1⁺ cells) was significantly enhanced compared to WT CO ($100.0 \pm 3.2\%$ Iba1⁺ cells, $p = 0.002$, **Figure 8D**) and KO CO ($107.2 \pm 6.4\%$ Iba1⁺ cells, $p < 0.05$) in peripheral regions of the retina. Also, the number of Iba1⁺ cells was lower in KO ONA ($85.1 \pm 3.1\%$ Iba1⁺ cells) compared to KO CO ($p < 0.01$) and WT CO ($p = 0.08$) in the periphery. Additionally, a significantly reduced microglial response was detected in immunized KO and WT animals ($p < 0.001$). Regarding the quantification of Iba1⁺

cells in the periphery, both control groups had similar cell counts ($p = 0.63$).

In the next step, RT-qPCR was used to investigate whether microglia have reactive phenotypes. Besides *Iba1*, we also examined the markers *Nos2* and *Cd68* in retinal tissue (**Figures 8E–G, Supplementary Table 5**). No differences could be detected in the *Iba1* expression between control WT and KO mice (1.3-fold, $p = 0.2$, **Figure 8E**). However, KO CO mice showed significantly elevated levels of *Nos2* (1.7-fold; $p = 0.013$) and *Cd68* (1.3-fold; $p = 0.017$) compared to WT CO. The comparison of immunized and non-immunized WT illustrated a significantly increased expression of *Iba1* (1.5-fold, $p = 0.048$) as well as of the reactive markers *Nos2* (1.4-fold, $p = 0.021$) and *Cd68* (1.3-fold, $p = 0.032$, **Figure 8F**). Interestingly, comparable expression levels of these microglial markers were found in immunized KO and KO CO (p

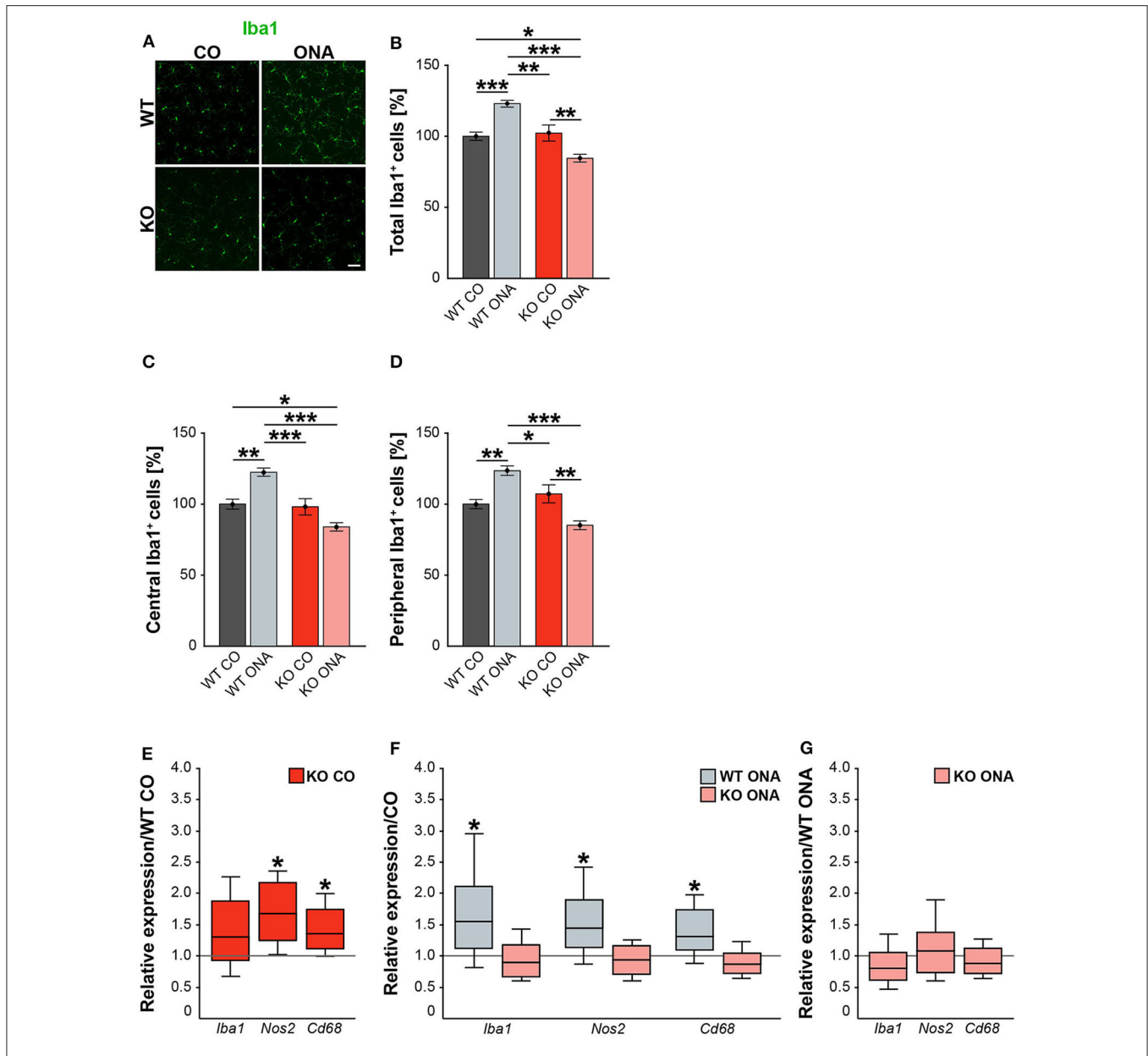


FIGURE 8 | Decreased microglia response after immunization in KO mice. **(A)** Representative pictures of Iba1⁺ cells (green) in retinal flat-mounts of immunized and non-immunized WT and KO mice. **(B–D)** Quantification of Iba1⁺ microglia in control and immunized WT and KO animals in the total, central and peripheral retina (*n* = 9/group). WT ONA group exhibited clearly more microglia. In contrast, KO ONA animals displayed fewer Iba1⁺ cells. **(E)** RT-qPCR analyses (*n* = 5/group) of the relative *Iba1*, *Nos2*, and *Cd68* mRNA expression showed a significant increase of *Nos2* and *Cd68* in KO CO compared to WT CO retinae. No differences were observed for *Iba1* mRNA expression. **(F)** Compared to WT CO, a significant upregulation of *Iba1*, *Nos2*, and *Cd68* levels were found in WT ONA. No significant changes were detected regarding the expression levels of these markers in KO ONA compared to KO CO. **(G)** After immunization, a comparable mRNA level of *Iba1*, *Cd68*, and *Nos2* was detected in KO ONA compared to WT ONA. Data were analyzed using two-way ANOVA followed by Tukey's *post-hoc* test and present as mean ± SEM in **(B–D)**. For RT-qPCR, groups were compared using the pairwise fixed reallocation and randomization test and were shown as median ± quartile ± minimum/maximum in **(E–G)**. **p* < 0.05; ***p* < 0.01; ****p* < 0.001. Scale bar = 50 μm.

> 0.05, **Figure 8F**). RT-qPCR analyses revealed comparable mRNA levels in KO ONA compared to WT ONA (*p* > 0.05, **Figure 8G**).

In line with the RT-qPCR results of retinal tissue, we found a similar expression pattern of microglial markers in

the optic nerve of control and immunized WT and KO mice (**Supplementary Table 5, Supplementary Figure 2**).

In summary, WT ONA animals showed a significantly increased microglia infiltration and glial marker expression, indicating an increased microglial response. Remarkably,

a significantly reduced invasion and reactivity of microglia were observed in KO ONA, suggesting that Tnc signaling is an important modulator of microglia in glaucomatous neurodegeneration.

Altered Expression Pattern of Pro- and Anti-inflammatory Cytokines in Immunized WT Compared to Immunized KO Animals

In our study, we noted a reactive gliosis and an increased microglial response after immunization in WT mice. Interestingly, these effects could not be detected in Tnc deficient animals.

Next, we analyzed the pro- and anti-inflammatory responses of the microglial phenotypes in retinae and optic nerves (**Figure 9, Supplementary Table 5**). Here, *Tnfa* was used to study M1 pro-inflammatory microglia, while *Tgfb1* is expressed by M2 anti-inflammatory microglia. RT-qPCR experiments revealed comparable mRNA level of *Tnfa* (1.4-fold, $p = 0.132$) and *Tgfb1* (1.4-fold, $p = 0.071$) in KO CO mice compared to WT CO mice (**Figure 9A**). After ONA-immunization, *Tnfa* was significantly upregulated in WT and interestingly downregulated in KO compared to the corresponding control groups (WT CO vs. WT ONA: 1.7-fold, $p = 0.026$ and KO CO vs. KO ONA: 0.4-fold, $p = 0.031$, **Figure 9B**). Statistical comparable *Tgfb1* mRNA levels were found in WT CO and WT ONA (1.0-fold; $p = 0.807$) as well as in KO CO and KO ONA (0.9-fold, $p = 0.415$; **Figure 9B**). The evaluation of both immunized genotypes showed a significant reduction of *Tnfa* (0.5-fold, $p = 0.036$) and a significant increase of *Tgfb1* (1.2-fold, $p = 0.005$) after immunization in KO mice (**Figure 9C**).

Finally, we examined, which microglial subtypes are altered due to an increased microglial reactivity in the optic nerve tissue of immunized and non-immunized WT and KO mice (**Figures 9D–F, Supplementary Table 5**). Equal mRNA levels of *Tnfa* (1.4-fold, $p = 0.07$) and *Tgfb1* (0.9-fold, $p = 0.659$) were seen in WT and KO controls (**Figure 9D**). A significantly enhanced *Tnfa* expression (2.1-fold, $p = 0.008$) and an unchanged *Tgfb1* expression (0.9-fold, $p = 0.71$) were detected in WT ONA compared to WT CO (**Figure 9E**). No changes of these markers were found in KO CO in comparison to KO ONA mice (*Tnfa*: 0.8-fold, $p = 0.443$ and *Tgfb1*: 0.9-fold, $p = 0.575$). In line with the RT-qPCR results of retinal tissue, we found a slightly reduced *Tnfa* (0.6-fold, $p = 0.101$) and an unaltered *Tgfb1* (0.8-fold, $p = 0.297$) expression between both immunized groups (**Figure 9F**).

In conclusion, missing Tnc resulted in a reduced mRNA level of pro-inflammatory *Tnfa*, but an enhanced expression of anti-inflammatory *Tgfb1*. The increased expression of the pro-inflammatory cytokine in WT after immunization points toward an enhanced presence of reactive M1 microglia.

DISCUSSION

Glaucoma involves a progressive degeneration of RGCs and their axons leading to visual field loss (62–64). Developing glaucoma is often associated with elevated IOP, but RGC damage can also occur without IOP changes. Previous studies

provided evidence that an altered immune response is involved in glaucoma pathology (2, 65–68). In addition, a remodeling of ECM constituents was found in several retinal neurodegenerative diseases, including glaucoma (31–33, 69, 70).

In glaucoma pathology the mechanisms are currently poorly understood, especially the relationship between RGC loss and the role of the immune system as well as ECM molecules. Hence, we characterized glaucomatous damage associated with the absence of the ECM glycoprotein Tnc in an IOP-independent EAG mouse model for the first time. Therefore, we immunized WT and KO mice with ONA to induce retinal damage and analyzed IOP, retinal functionality, RGC degeneration, glial activation, and pro- and anti-inflammatory cytokine expression.

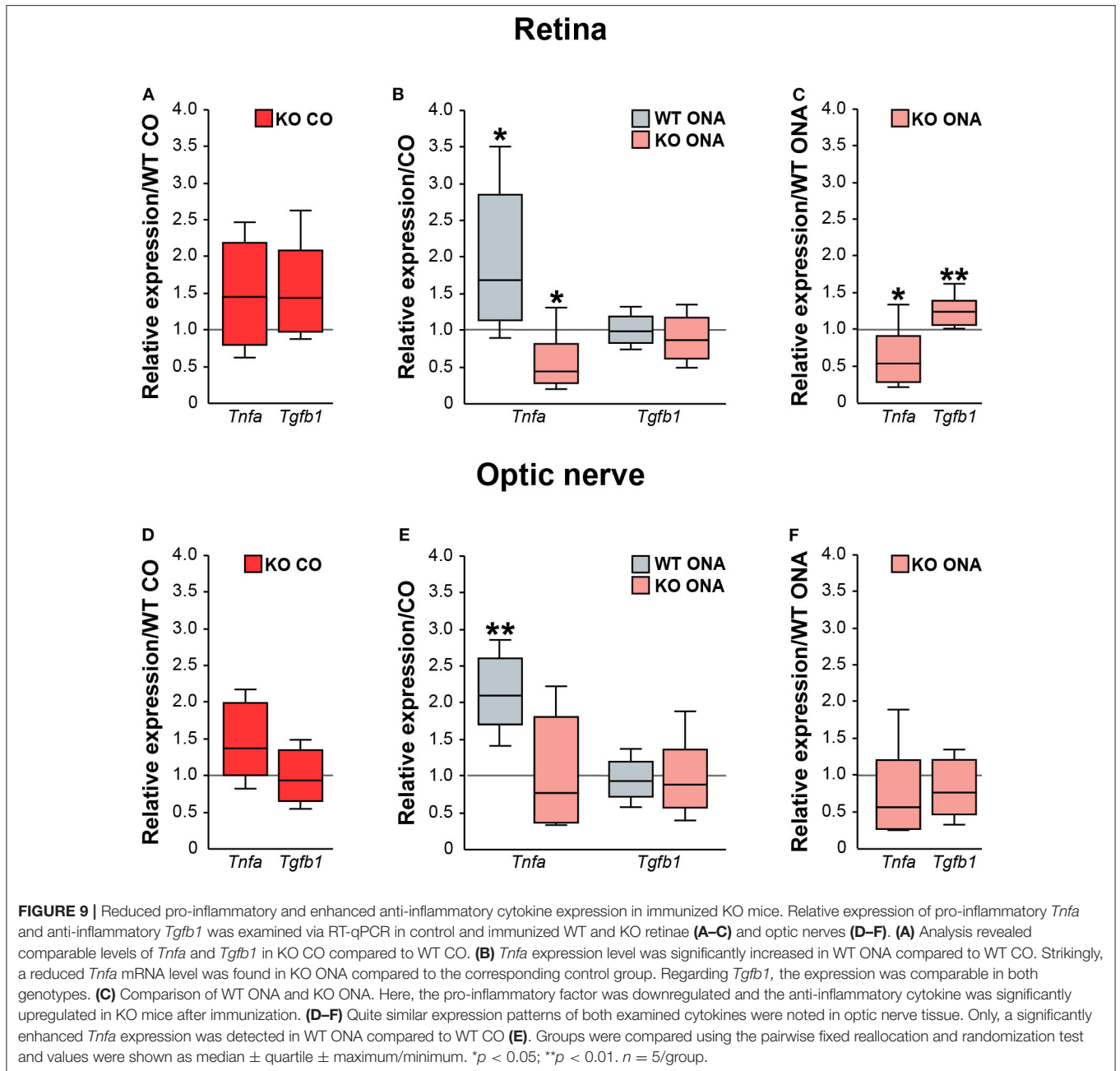
In a previous study, we already successfully transferred the EAG glaucoma model from rats to mice (49). Here, glaucomatous neurodegeneration was observed 6 weeks post ONA-immunization. However, in order to provoke a possible more robust glaucomatous macro- and microgliosis in our transgenic Tnc EAG mouse model, the duration of our study was extended to 10 weeks post immunization. Accordingly, we observed significantly increased GFAP levels and a higher number of Iba1⁺ infiltrating microglia cells in the WT, suggesting an induction of glaucomatous gliosis.

Our analyses revealed that the IOP of WT and KO stayed in normal ranges. Previous studies of the EAG animal model also showed no alteration in the IOP (49, 58). Comparable IOP in control and immunized animals points to the fact that the EAG model can be considered a suitable model for normal tension glaucoma.

Analyses of retinal functionality via ERG recordings revealed no differences in a- and b-wave responses in control and immunized WT and KO mice, which indicates that photoreceptor cells as well as bipolar and Müller glia cells are not affected in our model.

We found a significant loss of Brn3a⁺ RGCs in both genotypes following immunization. Interestingly, immunized KO mice displayed ~15% more RGCs in retinal flat-mounts compared to immunized WT mice. Moreover, a comparable number of RGCs was found in retinal cross-sections of KO ONA animals. We also verified a severe optic nerve damage by diminished β III-tubulin staining in immunized WT, while no alterations were found in the KO ONA mice. Previous studies of the EAG rat model showed that antibody deposits are accompanied by apoptotic RGC death (71). Furthermore, activation of the complement system via the lectin pathway seems to trigger retinal degeneration in this model (72). In our present study, we demonstrate that Tnc deficiency results in an extenuated loss of RGCs. Accordingly, we suggest that beside immunological alterations, Tnc-mediated signaling pathways are involved in glaucoma pathology.

In an EAG rat model a significant loss of RGCs could be detected 22 days after immunization (71). While an early upregulation of Tnc and its interaction partner RPTP β / ζ /phosphacan was observed already at 7 days (6). Additionally, we noted an increased Tnc immunoreactivity in the retina 14 days post immunization. However, we did not reveal any differences regarding the Tnc protein level at later



points in time, namely 28 days after immunization. Therefore, we assume that alterations of *Tnc* levels occurred at an early point in time, shortly after immunization and then returned to normal values. Due to the fact that glaucomatous degeneration in both rodent EAG models is temporally comparable, we also assume that *Tnc* induction takes place at similar points in time. However, the precise timeline of *Tnc* induction should be determined in a future follow-up project. Ten weeks after immunization, we observed *Tnc* immunoreactivity in horizontal and amacrine cells as well as in the outer and inner plexiform layers (27, 28). The quantification of the *Tnc* signal intensity revealed comparable protein levels in control and immunized WT mice. This is in line

with results from the EAG rat model, where no differences in the *Tnc* protein levels were noted at later points in time (6).

In regard to the temporal induction, *Tnc* expression levels were enhanced 3 days post injury and returned to normal levels 7 and 14 days after the induction of brain laser lesion (73). In the CNS, *Tnc* is re-expressed under pathological conditions and represents an important component of the glial scar (11, 25, 36, 74–76). In Alzheimer's disease, *Tnc* immunoreactivity is highly associated with amyloid- β plaques (20). In multiple sclerosis, *Tnc* has an immunomodulatory function and loss of *Tnc* protects from experimental autoimmune encephalopathy (24). In regard to brain injury it was demonstrated that *Tnc*

isoforms that contain the fibronectin type III domains B and D as well as the smallest splice variants, were specifically upregulated after cortical lesion (77). Future studies should focus on comprehensive analyses of specific Tnc isoforms in our glaucoma model. Due to these and our results, we conclude that Tnc induction occurred at early points in time and returned to normal levels at later points in time after immunization with ocular antigens. We speculate that upregulation of Tnc may serve as an early indicator for neurodegenerative processes before retinal damage is detectable. Finally, we assume that Tnc is a key mediator of inflammatory responses in our glaucoma mouse model.

Studies reported that Tnc is involved in the pathogenesis of CNS autoimmunity and astrocytes are a main Tnc source (24, 29, 30, 34–36). Astrocytes are the major glial cells in the optic nerve head and provide neurotrophic as well as mechanical support for RGC axons. Furthermore, astrocytes influence survival and functionality of neurons (78, 79). Neuroinflammatory processes, characterized by altered functional properties and distribution of glial cells, appear to have an obvious function in glaucomatous optic neuropathy (80–82). In addition, an enhanced astrocyte reactivity in response to inflammatory signals is directly regulated by the ECM (83). Furthermore, RGC degeneration is accompanied by reactive astrogliosis, which results in a higher GFAP expression (51, 58, 84–86). In our study, we observed an upregulated *Gfap* expression and an increased GFAP immunostaining in retinal and optic nerve tissue of immunized WT mice, whereas absence of Tnc led to a missing reactive gliosis. Therefore, severe glaucomatous damage induced by immunization seems to be triggered by Tnc expressing reactive astrocytes in the WT condition. We assume that the increase of astrocytic Tnc results in an enhanced glial cell proliferation, infiltration and cytokine release.

We noted a reduced population of mature oligodendrocytes and OPCs after immunization in WT mice. Also, a reduced MBP immunoreactivity demonstrated a demyelination of the optic nerve in the WT condition. Furthermore, no evidence of a decreased oligodendroglia density and demyelination was detected after ONA-immunization in KO animals. Interestingly, the fraction of mature Olig2/CC1 double immunopositive oligodendrocytes was significantly increased in the KO, in agreement with findings that Tnc inhibits the maturation of oligodendrocytes (17, 87). In addition, a strong expression of Tnc in the optic nerve head inhibits the migration of oligodendrocytes from the optic nerve into the retina (88). Based on our results and the mentioned studies, we suggest that Tnc has an impact on demyelination processes. Missing of Tnc leads to no alteration in oligodendroglia but has a protective effect on myelination of optic nerve fibers in our EAG mouse model.

Microglia are the main resident immune cells of the CNS and play a crucial role during retinal neurodegeneration (89). They change their morphology to a reactive amoeboid cell type after injury and neuroinflammatory changes in the retina occur during glaucomatous damage (81). Microglial activation is a very early event in glaucoma, often before significant loss of RGCs takes place (47, 90, 91). Analyses of microglial cells showed that Tnc deficiency results in a diminished

microglial response characterized by a reduced number and reactivity. Furthermore, we detected enhanced levels of the anti-inflammatory factor *Tgfb1* and a decreased expression of the pro-inflammatory *Tnfa*. This is consistent with the study by Piccinini, which demonstrated that the deletion of Tnc reduced TNF- α production (92). In the retina, TGF- β signaling has an important role in neuronal differentiation and survival (93). In microglia, TGF- β regulates homeostasis and lack of TGF- β signaling promotes retinal degeneration (94, 95). Additionally, TGF- β inhibits pro-inflammatory cytokines and regulates proliferation and activity of microglia (96). Our results indicate that the loss of Tnc signaling in microglia may promote the neuroprotective M2-subtype, resulting in a weaker RGC loss as well as axonal fiber damage in immunized KO animals.

The WT condition exhibited unaltered *Tgfb1* expression and it is known that Tnc is able to bind this growth factor (97). In a pilocarpine seizure model it was shown that TGF- β signaling is accompanied by Tnc upregulation (98). Here, an increase of the *Tgfb1* level occurred shortly after pilocarpine application, whereas the rise of *Tgfb1* was less pronounced over time. Based on this date, we suggest that TGF- β dependent signaling in WT mice is associated with an early upregulation of Tnc and becomes less efficient at later points in time.

An enhanced microglial infiltration and marker expression revealed an increased glial response in WT post immunization in our study. Moreover, we found a significantly increased expression of the pro-inflammatory cytokine *Tnfa*. In glaucoma, a glia-derived neuronal death was described through TNF- α (99–102). The indirect neurotoxicity of this pro-inflammatory factor is based on TNF receptor 2-mediated activation of microglia, whereas blocking of TNF- α results in an extenuated microglial response (101). Moreover, TNF- α does not directly induce RGC death but leads to an upregulation of the microglial Fas ligand, where the membrane-bound form elicits RGC apoptosis (103, 104). However, in an early phase after injury a neuroprotective effect of TNF- α was found in an optic nerve crush animal model (105).

Microglia are involved in time-dependent astrocytic reactivity and this cross-talk is mediated by cytokines such as TNF- α (106–108). Previous studies noted that resting microglia switched to a M1-like phenotype, which can lead to neurotoxic effects by producing high levels of pro-inflammatory cytokines (43, 109, 110). Based on this, we speculate that microglia are the first glial cells that react after immunization as a driving force of reactive gliosis in the EAG mouse model. Our investigations of immunized WT and Tnc deficient mice lead to the assumption that Tnc promotes immunomodulatory processes of the neurotoxic M1-subtype in turns of higher activity. This is in line with previous reports that Tnc supports the activity of M1-microglia (36, 111).

Astrocytes as well as microglia express the toll-like receptor 4 (TLR4) and its expression is maintained by the extracellular environment (112, 113). Tnc activates TLR4 via its fibrinogen-like globe domain and thereby regulates the production of pro-inflammatory cytokines, such as IL-6, IL-8, and TNF- α (114, 115). In primary microglia, Tnc induced the synthesis of *Tnfa* and regulated the expression of *iNOS* via TLR4

signaling (38). Besides microglia, activated macrophages can also produce TNF- α (116). In human macrophages, specific alternatively spliced *Tnc* isoforms stimulate IL-6 and TNF- α release via TLR4 activation (117). In an experimental model of retinal degeneration, infiltration of peripheral monocytes occurred very early on, before microglia activation could be observed (118). Accordingly, we conclude that enhanced *Tnfa* expression, 10 weeks after immunization, is caused by *Tnc*-induced microglial TLR4 activation. Furthermore, we speculate that microglial TNF- α release and *Tnc* itself may regulate astrocytic *Tnc* expression, which results in a subsequently harmful astrogliosis in glaucomatous WT mice.

Our study could show that *Tnc* signaling pathways modulate both microglia and astrocyte response during glaucomatous damage. This might lead to a feedback loop by which increased levels of M1-microglial factors impact astrocytic *Tnc* release and vice versa. Finally, we propose that *Tnc* acts as an endogenous TLR4 ligand and represents an alarmin in our glaucoma model. However, it is possible that other receptors, for instance integrins, have an impact on inflammatory effects of *Tnc* (119, 120). In this regard, also other ECM components and *Tnc* interaction partners might be involved. Here, e.g., the extra domain A of fibronectin was recently described to elevate IOP through TLR4 signaling in a TGF β 2-induced ocular hypertension mouse model (121). Hence, future studies should focus on the downstream signaling cascade of TLR4 in our IOP-independent EAG mouse model.

CONCLUSION

Taken together, our study demonstrated that *Tnc* influences glial response, migration, and inflammation during glaucomatous damage. This model is ideally suited for a better understanding of the molecular mechanisms between retinal neurodegeneration and ECM remodeling in order to develop future therapeutic options.

REFERENCES

- Tezel G, Seigel GM, Wax MB. Autoantibodies to small heat shock proteins in glaucoma. *Invest Ophthalmol Vis Sci.* (1998) 39:2277–87.
- Wax MB, Yang J, Tezel G. Serum autoantibodies in patients with glaucoma. *J Glaucoma.* (2001) 10:S22–24. doi: 10.1097/00061198-20011001-00009
- Wax MB. The case for autoimmunity in glaucoma. *Exp Eye Res.* (2011) 93:187–90. doi: 10.1016/j.exer.2010.08.016
- Laspar P, Gramlich OW, Muller HD, Cuny CS, Gottschling PF, Pfeiffer N, et al. Autoreactive antibodies and loss of retinal ganglion cells in rats induced by immunization with ocular antigens. *Invest Ophthalmol Vis Sci.* (2011) 52:8835–48. doi: 10.1167/iovs.10-6889
- Joachim SC, Reinehr S, Kuehn S, Laspar P, Gramlich OW, Kuehn M, et al. Immune response against ocular tissues after immunization with optic nerve antigens in a model of autoimmune glaucoma. *Mol Vis.* (2013) 19:1804–14.
- Reinehr S, Reinhard J, Wiemann S, Stute G, Kuehn S, Woestmann J, et al. Early remodelling of the extracellular matrix proteins tenascin-C and phosphacan in retina and optic nerve of an experimental autoimmune glaucoma model. *J Cell Mol Med.* (2016) 20:2122–37. doi: 10.1111/jcmm.12909
- Hynes RO. The extracellular matrix: not just pretty fibrils. *Science.* (2009) 326:1216–9. doi: 10.1126/science.1176009
- Theocharidis U, Long K, Ffrench-Constant C, Faissner A. Regulation of the neural stem cell compartment by extracellular matrix constituents. *Prog Brain Res.* (2014) 214:3–28. doi: 10.1016/B978-0-444-63486-3.00001-3
- Faissner A, Reinhard J. The extracellular matrix compartment of neural stem and glial progenitor cells. *Glia.* (2015) 63:1330–49. doi: 10.1002/glia.22839
- Krishnaswamy VR, Benbenishty A, Blinder P, Sagi I. Demystifying the extracellular matrix and its proteolytic remodeling in the brain: structural and functional insights. *Cell Mol Life Sci.* (2019) 76:3229–48. doi: 10.1007/s00018-019-03182-6
- Roll L, Faissner A. Tenascins in CNS lesions. *Semin Cell Dev Biol.* (2019) 89:118–24. doi: 10.1016/j.semcdb.2018.09.012
- Theocharis AD, Manou D, Karamanos NK. The extracellular matrix as a multitasking player in disease. *FEBS J.* (2019) 286:2830–69. doi: 10.1111/febs.14818

DATA AVAILABILITY STATEMENT

All datasets generated for this study are included in the article/**Supplementary Material**.

ETHICS STATEMENT

The animal study was reviewed and approved by Landesamt für Natur, Umwelt und Verbraucherschutz, North Rhine-Westphalia.

AUTHOR CONTRIBUTIONS

SW performed experiments, analyzed data, and wrote the manuscript. JR designed the study, analyzed data, and revised the manuscript. SR and ZC performed experiments and analyzed data. SCJ and AF designed the study and revised the manuscript. All authors read and approved the final manuscript.

FUNDING

AF received grant support from the German Research Foundation (DFG, FA-159/24-1). SW was supported by the Konrad-Adenauer-Foundation (200520593).

ACKNOWLEDGMENTS

This manuscript has been released as a pre-print at bioRxiv, (122). The authors thank Stephanie Chun, Anja Coenen, Sabine Kindermann, Franziska Mennes, Annalena Pamp, and Marion Voelzkow for excellent technical assistance.

SUPPLEMENTARY MATERIAL

The Supplementary Material for this article can be found online at: <https://www.frontiersin.org/articles/10.3389/fimmu.2020.566279/full#supplementary-material>

13. Garcion E, Faissner A, Ffrench-Constant C. Knockout mice reveal a contribution of the extracellular matrix molecule tenascin-C to neural precursor proliferation and migration. *Development*. (2001) 128:2485–96.
14. Joester A, Faissner A. The structure and function of tenascins in the nervous system. *Matrix Biol*. (2001) 20:13–22. doi: 10.1016/S0945-053X(00)00136-0
15. Garwood J, Garcion E, Dobbertin A, Heck N, Calco V, Ffrench-Constant C, et al. The extracellular matrix glycoprotein Tenascin-C is expressed by oligodendrocyte precursor cells and required for the regulation of maturation rate, survival and responsiveness to platelet-derived growth factor. *Eur J Neurosci*. (2004) 20:2524–40. doi: 10.1111/j.1460-9568.2004.03727.x
16. Loers G, Schachner M. Recognition molecules and neural repair. *J Neurochem*. (2007) 101:865–82. doi: 10.1111/j.1471-4159.2006.04409.x
17. Czopka T, Von Holst A, Ffrench-Constant C, Faissner A. Regulatory mechanisms that mediate tenascin C-dependent inhibition of oligodendrocyte precursor differentiation. *J Neurosci*. (2010) 30:12310–22. doi: 10.1523/JNEUROSCI.4957-09.2010
18. Rigato F, Garwood J, Calco V, Heck N, Faivre-Sarrailh C, Faissner A. Tenascin-C promotes neurite outgrowth of embryonic hippocampal neurons through the alternatively spliced fibronectin type III BD domains via activation of the cell adhesion molecule F3/contactin. *J Neurosci*. (2002) 22:6596–609. doi: 10.1523/JNEUROSCI.22-15-06596.2002
19. Faissner A, Roll L, Theoharidis U. Tenascin-C in the matrisome of neural stem and progenitor cells. *Mol Cell Neurosci*. (2017) 81:22–31. doi: 10.1016/j.mcn.2016.11.003
20. Mi Z, Halfter W, Abrahamson EE, Klunk WE, Mathis CA, Mufson EJ, et al. Tenascin-C is associated with cored amyloid-beta plaques in Alzheimer disease and pathology burdened cognitively normal elderly. *J Neuropathol Exp Neurol*. (2016) 75:868–76. doi: 10.1093/jnen/nlw062
21. Xie K, Liu Y, Hao W, Walter S, Penke B, Hartmann T, et al. Tenascin-C deficiency ameliorates Alzheimer's disease-related pathology in mice. *Neurobiol Aging*. (2013) 34:2389–98. doi: 10.1016/j.neurobiolaging.2013.04.013
22. Ruhmann M, Piccinini AM, Kong PL, Midwood KS. Endogenous activation of adaptive immunity: tenascin-C drives interleukin-17 synthesis in murine arthritic joint disease. *Arthritis Rheum*. (2012) 64:2179–90. doi: 10.1002/art.34401
23. Machino-Ohtsuka T, Tajiri K, Kimura T, Sakai S, Sato A, Yoshida T, et al. Tenascin-C aggravates autoimmune myocarditis via dendritic cell activation and Th17 cell differentiation. *J Am Heart Assoc*. (2014) 3:e001052. doi: 10.1161/JAHA.114.001052
24. Momcilovic M, Stamenkovic V, Jovanovic M, Andjus PR, Jakovcevski I, Schachner M, et al. Tenascin-C deficiency protects mice from experimental autoimmune encephalomyelitis. *J Neuroimmunol*. (2017) 302:1–6. doi: 10.1016/j.jneuroim.2016.12.001
25. Reinhard J, Roll L, Faissner A. Tenascins in retinal and optic nerve neurodegeneration. *Front Integr Neurosci*. (2017) 11:30. doi: 10.3389/fnint.2017.00030
26. Klausmeyer A, Garwood J, Faissner A. Differential expression of phosphacan/RPTPbeta isoforms in the developing mouse visual system. *J Comp Neurol*. (2007) 504:659–79. doi: 10.1002/cne.21479
27. D'alessandri L, Ranscht B, Winterhalter KH, Vaughan L. Contactin/F11 and tenascin-C co-expression in the chick retina correlates with formation of the synaptic plexiform layers. *Curr Eye Res*. (1995) 14:911–26. doi: 10.3109/02713689508995131
28. Sanchez-Lopez A, Cuadros MA, Calvente R, Tassi M, Marin-Teva JL, Navascues J. Radial migration of developing microglial cells in quail retina: a confocal microscopy study. *Glia*. (2004) 46:261–73. doi: 10.1002/glia.20007
29. Bartsch U, Pesheva P, Raff M, Schachner M. Expression of janusin. (J1-160/180) in the retina and optic nerve of the developing and adult mouse. *Glia*. (1993) 9:57–69. doi: 10.1002/glia.440090108
30. Reinhard J, Joachim SC, Faissner A. Extracellular matrix remodeling during retinal development. *Exp Eye Res*. (2015) 133:132–40. doi: 10.1016/j.exer.2014.07.001
31. Reinhard J, Renner M, Wiemann S, Shakoor DA, Stute G, Dick HB, et al. Ischemic injury leads to extracellular matrix alterations in retina and optic nerve. *Sci Rep*. (2017) 7:43470. doi: 10.1038/srep43470
32. Johnson EC, Jia L, Cepurna WO, Doser TA, Morrison JC. Global changes in optic nerve head gene expression after exposure to elevated intraocular pressure in a rat glaucoma model. *Invest Ophthalmol Vis Sci*. (2007) 48:3161–77. doi: 10.1167/iovs.06-1282
33. Pena JD, Varela HJ, Ricard CS, Hernandez MR. Enhanced tenascin expression associated with reactive astrocytes in human optic nerve heads with primary open angle glaucoma. *Exp Eye Res*. (1999) 68:29–40. doi: 10.1006/exer.1998.0577
34. Jakovcevski I, Miljkovic D, Schachner M, Andjus PR. Tenascins and inflammation in disorders of the nervous system. *Amino Acids*. (2013) 44:1115–27. doi: 10.1007/s00726-012-1446-0
35. Dzyubenko E, Manrique-Castano D, Kleinschnitz C, Faissner A, Hermann DM. Role of immune responses for extracellular matrix remodeling in the ischemic brain. *Ther Adv Neurol Disord*. (2018) 11:1756286418818092. doi: 10.1177/1756286418818092
36. Wiemann S, Reinhard J, Faissner A. Immunomodulatory role of the extracellular matrix protein tenascin-C in neuroinflammation. *Biochem Soc Trans*. (2019) 47:1651–60. doi: 10.1042/BST20190081
37. Smith GM, Hale JH. Macrophage/Microglia regulation of astrocytic tenascin: synergistic action of transforming growth factor-beta and basic fibroblast growth factor. *J Neurosci*. (1997) 17:9624–33. doi: 10.1523/JNEUROSCI.17-24-09624.1997
38. Haage V, Elmadany N, Roll L, Faissner A, Gutmann DH, Semtner M, et al. Tenascin C regulates multiple microglial functions involving TLR4 signaling and HDAC1. *Brain Behav Immun*. (2019) 81:1–672. doi: 10.1016/j.bbi.2019.06.047
39. Glass CK, Saijo K, Winner B, Marchetto MC, Gage FH. Mechanisms underlying inflammation in neurodegeneration. *Cell*. (2010) 140:918–34. doi: 10.1016/j.cell.2010.02.016
40. Langmann T. Microglia activation in retinal degeneration. *J Leukoc Biol*. (2007) 81:1345–51. doi: 10.1189/jlb.0207114
41. Wolf SA, Boddeke HW, Kettenmann H. Microglia in Physiology and Disease. *Annu Rev Physiol*. (2017) 79:619–43. doi: 10.1146/annurev-physiol-022516-034406
42. Harms AS, Lee JK, Nguyen TA, Chang J, Ruhn KM, Trevino I, et al. Regulation of microglia effector functions by tumor necrosis factor signaling. *Glia*. (2012) 60:189–202. doi: 10.1002/glia.21254
43. Varnum MM, Ikezu T. The classification of microglial activation phenotypes on neurodegeneration and regeneration in Alzheimer's disease brain. *Arch Immunol Ther Exp*. (2012) 60:251–66. doi: 10.1007/s00005-012-0181-2
44. Silverman SM, Wong WT. Microglia in the retina: roles in development, maturity, and disease. *Annu Rev Vis Sci*. (2018) 4:45–77. doi: 10.1146/annurev-vision-091517-034425
45. De Simone R, Ajmone-Cat MA, Minghetti L. Atypical antiinflammatory activation of microglia induced by apoptotic neurons: possible role of phosphatidylserine-phosphatidylserine receptor interaction. *Mol Neurobiol*. (2004) 29:197–212. doi: 10.1385/MN:29:2:197
46. Colton CA. Heterogeneity of microglial activation in the innate immune response in the brain. *J Neuroimmune Pharmacol*. (2009) 4:399–418. doi: 10.1007/s11481-009-9164-4
47. Ramirez AI, De Hoz R, Salobrar-Garcia E, Salazar JJ, Rojas B, Ajoy D, et al. The Role of Microglia in Retinal Neurodegeneration: Alzheimer's Disease, Parkinson, and Glaucoma. *Front Aging Neurosci*. (2017) 9:214. doi: 10.3389/fnagi.2017.00214
48. Forsberg E, Hirsch E, Frohlich L, Meyer M, Ekblom P, Aszodi A, et al. Skin wounds and severed nerves heal normally in mice lacking tenascin-C. *Proc Natl Acad Sci USA*. (1996) 93:6594–9. doi: 10.1073/pnas.93.13.6594
49. Reinehr S, Reinhard J, Wiemann S, Hesse K, Voss C, Gandej M, et al. Transfer of the experimental autoimmune glaucoma model from rats to mice—new options to study glaucoma disease. *Int J Mol Sci*. (2019) 20. doi: 10.3390/ijms20102563
50. Schmid H, Renner M, Dick HB, Joachim SC. Loss of inner retinal neurons after retinal ischemia in rats. *Invest Ophthalmol Vis Sci*. (2014) 55:2777–87. doi: 10.1167/iovs.13-13372
51. Reinhard J, Wiemann S, Joachim SC, Palmhof M, Woestmann J, Denecke B, et al. Heterozygous Meg2 ablation causes intraocular pressure elevation and progressive glaucomatous neurodegeneration. *Mol Neurobiol*. (2019) 56:4322–45. doi: 10.1007/s12035-018-1376-2

52. Faissner A, Kruse J. J1/tenascin is a repulsive substrate for central nervous system neurons. *Neuron*. (1990) 5:627–37. doi: 10.1016/0896-6273(90)90217-4
53. Reinehr S, Kuehn S, Casola C, Koch D, Stute G, Grotegut P, et al. HSP27 immunization reinforces AII amacrine cell and synapse damage induced by S100 in an autoimmune glaucoma model. *Cell Tissue Res*. (2018) 371:237–49. doi: 10.1007/s00441-017-2710-0
54. Xiang M, Zhou H, Nathans J. Molecular biology of retinal ganglion cells. *Proc Natl Acad Sci USA*. (1996) 93:596–601. doi: 10.1073/pnas.93.2.596
55. Nadal-Nicolas FM, Jimenez-Lopez M, Sobrado-Calvo P, Nieto-Lopez L, Canovas-Martinez I, Salinas-Navarro M, et al. Brn3a as a marker of retinal ganglion cells: qualitative and quantitative time course studies in naive and optic nerve-injured retinas. *Invest Ophthalmol Vis Sci*. (2009) 50:3860–8. doi: 10.1167/iovs.08-3267
56. Ito D, Imai Y, Ohsawa K, Nakajima K, Fukuuchi Y, Kohsaka S. Microglia-specific localisation of a novel calcium binding protein, Iba1. *Brain Res Mol Brain Res*. (1998) 57:1–9. doi: 10.1016/S0169-328X(98)00040-0
57. Pfaffl MW, Horgan GW, Dempfle L. Relative expression software tool. (REST) for group-wise comparison and statistical analysis of relative expression results in real-time PCR. *Nucleic Acids Res*. (2002) 30:e36. doi: 10.1093/nar/30.9.e36
58. Noristani R, Kuehn S, Stute G, Reinehr S, Stellbogen M, Dick HB, et al. Retinal and optic nerve damage is associated with early glial responses in an experimental autoimmune glaucoma model. *J Mol Neurosci*. (2016) 58:470–82. doi: 10.1007/s12031-015-0707-2
59. Gautier HO, Evans KA, Vollbracht K, James R, Sitnikov S, Lundgaard I, et al. Neuronal activity regulates remyelination via glutamate signalling to oligodendrocyte progenitors. *Nat Commun*. (2015) 6:8518. doi: 10.1038/ncomms9518
60. Bin JM, Harris SN, Kennedy TE. The oligodendrocyte-specific antibody 'CC1' binds Quaking 7. *J Neurochem*. (2016) 139:181–6. doi: 10.1111/jnc.13745
61. Pohl HB, Porcheri C, Mueggler T, Bachmann LC, Martino G, Riethmacher D, et al. Genetically induced adult oligodendrocyte cell death is associated with poor myelin clearance, reduced remyelination, and axonal damage. *J Neurosci*. (2011) 31:1069–80. doi: 10.1523/JNEUROSCI.5035-10.2011
62. Tochel CM, Morton JS, Jay JL, Morrison JD. Relationship between visual field loss and contrast threshold elevation in glaucoma. *BMC Ophthalmol*. (2005) 5:22. doi: 10.1186/1471-2415-5-22
63. Shon K, Wollstein G, Schuman JS, Sung KR. Prediction of glaucomatous visual field progression: pointwise analysis. *Curr Eye Res*. (2014) 39:705–10. doi: 10.3109/02713683.2013.867353
64. Mcmonnies CW. Glaucoma history and risk factors. *J Optom*. (2017) 10:71–8. doi: 10.1016/j.optom.2016.02.003
65. Wax MB, Tezel G, Edward PD. Clinical and ocular histopathological findings in a patient with normal-pressure glaucoma. *Arch Ophthalmol*. (1998) 116:993–1001. doi: 10.1001/archoph.116.8.993
66. Tezel G, Edward DP, Wax MB. Serum autoantibodies to optic nerve head glycosaminoglycans in patients with glaucoma. *Arch Ophthalmol*. (1999) 117:917–24. doi: 10.1001/archoph.117.7.917
67. Joachim SC, Grus FH, Pfeiffer N. Analysis of autoantibody repertoires in sera of patients with glaucoma. *Eur J Ophthalmol*. (2003) 13:752–8. doi: 10.1177/1120672103013009-1003
68. Grus FH, Joachim SC, Bruns K, Lackner KJ, Pfeiffer N, Wax MB. Serum autoantibodies to alpha-fodrin are present in glaucoma patients from Germany and the United States. *Invest Ophthalmol Vis Sci*. (2006) 47:968–76. doi: 10.1167/iovs.05-0685
69. Hernandez MR, Andrzejewska WM, Neufeld AH. Changes in the extracellular matrix of the human optic nerve head in primary open-angle glaucoma. *Am J Ophthalmol*. (1990) 109:180–8. doi: 10.1016/S0002-9394(14)75984-7
70. Hernandez MR. Ultrastructural immunocytochemical analysis of elastin in the human lamina cribrosa. changes in elastic fibers in primary open-angle glaucoma. *Invest Ophthalmol Vis Sci*. (1992) 33:2891–903.
71. Joachim SC, Mondon C, Gramlich OW, Grus FH, Dick HB. Apoptotic retinal ganglion cell death in an autoimmune glaucoma model is accompanied by antibody depositions. *J Mol Neurosci*. (2014) 52:216–24. doi: 10.1007/s12031-013-0125-2
72. Reinehr S, Reinhard J, Gandej M, Kuehn S, Noristani R, Faissner A, et al. Simultaneous complement response via lectin pathway in retina and optic nerve in an experimental autoimmune glaucoma model. *Front Cell Neurosci*. (2016) 10:140. doi: 10.3389/fncel.2016.00140
73. Roll L, Eysel UT, Faissner A. Laser lesion in the mouse visual cortex induces a stem cell niche-like extracellular matrix, produced by immature astrocytes. *Front Cell Neurosci*. (2020) 14:102. doi: 10.3389/fncel.2020.00102
74. Fawcett JW, Asher RA. The glial scar and central nervous system repair. *Brain Res Bull*. (1999) 49:377–91. doi: 10.1016/S0361-9230(99)00072-6
75. Roll L, Mittmann T, Eysel UT, Faissner A. The laser lesion of the mouse visual cortex as a model to study neural extracellular matrix remodeling during degeneration, regeneration and plasticity of the CNS. *Cell Tissue Res*. (2012) 349:133–45. doi: 10.1007/s00441-011-1313-4
76. Bradbury EJ, Burnside ER. Moving beyond the glial scar for spinal cord repair. *Nat Commun*. (2019) 10:3879. doi: 10.1038/s41467-019-11707-7
77. Dobbertin A, Czvitkovich S, Theodoridis U, Garwood J, Andrews MR, Properzi F, et al. Analysis of combinatorial variability reveals selective accumulation of the fibronectin type III domains B and D of tenascin-C in injured brain. *Exp Neurol*. (2010) 225:60–73. doi: 10.1016/j.expneurol.2010.04.019
78. Russo R, Varano GP, Adornetto A, Nucci C, Corasaniti MT, Bagetta G, et al. Retinal ganglion cell death in glaucoma: Exploring the role of neuroinflammation. *Eur J Pharmacol*. (2016) 787:134–42. doi: 10.1016/j.ejphar.2016.03.064
79. De Hoz R, Rojas B, Ramirez AI, Salazar JJ, Gallego BI, Trivino A, et al. Retinal macroglial responses in health and disease. *Biomed Res Int*. (2016) 2016:2954721. doi: 10.1155/2016/2954721
80. Soto I, Howell GR. The complex role of neuroinflammation in glaucoma. *Cold Spring Harb Perspect Med*. (2014) 4. doi: 10.1101/cshperspect.a017269
81. Williams PA, Marsh-Armstrong N, Howell GR, Lasker IIOA, Glaucomatous Neurodegeneration P. Neuroinflammation in glaucoma: a new opportunity. *Exp Eye Res*. (2017) 157:20–7. doi: 10.1016/j.exer.2017.02.014
82. Melik Parsadaniant S, Reaux-Le Goazigo A, Sapienza A, Habas C, Baudouin C. Glaucoma: a degenerative optic neuropathy related to neuroinflammation? *Cells*. (2020) 9:535. doi: 10.3390/cells9030535
83. Johnson KM, Milner R, Crocker SJ. Extracellular matrix composition determines astrocyte responses to mechanical and inflammatory stimuli. *Neurosci Lett*. (2015) 600:104–9. doi: 10.1016/j.neulet.2015.06.013
84. Senatorov V, Malyukova I, Fariss R, Wawrousek EF, Swaminathan S, Sharan SK, et al. Expression of mutated mouse myocilin induces open-angle glaucoma in transgenic mice. *J Neurosci*. (2006) 26:11903–14. doi: 10.1523/JNEUROSCI.3020-06.2006
85. Inman DM, Horner PJ. Reactive nonproliferative gliosis predominates in a chronic mouse model of glaucoma. *Glia*. (2007) 55:942–53. doi: 10.1002/glia.20516
86. Johnson EC, Morrison JC. Friend or foe? Resolving the impact of glial responses in glaucoma. *J Glaucoma*. (2009) 18:341–53. doi: 10.1097/IJG.0b013e31818c6ef6
87. Czopka T, Von Holst A, Schmidt G, Ffrench-Constant C, Faissner A. Tenascin C and tenascin R similarly prevent the formation of myelin membranes in a RhoA-dependent manner, but antagonistically regulate the expression of myelin basic protein via a separate pathway. *Glia*. (2009) 57:1790–801. doi: 10.1002/glia.20891
88. Bartsch U, Faissner A, Trotter J, Dorries U, Bartsch S, Mohajeri H, et al. Tenascin demarcates the boundary between the myelinated and nonmyelinated part of retinal ganglion cell axons in the developing and adult mouse. *J Neurosci*. (1994) 14:4756–68. doi: 10.1523/JNEUROSCI.14-08-04756.1994
89. Rashid K, Akhtar-Schaefer I, Langmann T. Microglia in retinal degeneration. *Front Immunol*. (2019) 10:1975. doi: 10.3389/fimmu.2019.01975
90. Ebner A, Casson RJ, Wood JP, Chidlow G. Microglial activation in the visual pathway in experimental glaucoma: spatiotemporal characterization and correlation with axonal injury. *Invest Ophthalmol Vis Sci*. (2010) 51:6448–60. doi: 10.1167/iovs.10-5284
91. Bosco A, Steele MR, Vetter ML. Early microglia activation in a mouse model of chronic glaucoma. *J Comp Neurol*. (2011) 519:599–620. doi: 10.1002/cne.22516

92. Piccinini AM, Midwood KS. Endogenous control of immunity against infection: tenascin-C regulates TLR4-mediated inflammation via microRNA-155. *Cell Rep.* (2012) 2:914–26. doi: 10.1016/j.celrep.2012.09.005
93. Braunger BM, Pielmeier S, Demmer C, Landstorfer V, Kawall D, Abramov N, et al. TGF-beta signaling protects retinal neurons from programmed cell death during the development of the mammalian eye. *J Neurosci.* (2013) 33:14246–58. doi: 10.1523/JNEUROSCI.0991-13.2013
94. Zoller T, Schneider A, Kleimeyer C, Masuda T, Potru PS, Pfeifer D, et al. Silencing of TGFbeta signalling in microglia results in impaired homeostasis. *Nat Commun.* (2018) 9:4011. doi: 10.1038/s41467-018-06224-y
95. Ma W, Silverman SM, Zhao L, Villasmil R, Campos MM, Amaral J, et al. Absence of TGFbeta signaling in retinal microglia induces retinal degeneration and exacerbates choroidal neovascularization. *Elife.* (2019) 8. doi: 10.7554/eLife.42049
96. Piras F, Salani F, Bossu P, Caltagirone C, Spalletta G. High serum levels of transforming growth factor beta1 are associated with increased cortical thickness in cingulate and right frontal areas in healthy subjects. *J Neuroinflammation.* (2012) 9:42. doi: 10.1186/1742-2094-9-42
97. De Laporte L, Rice JJ, Tortelli F, Hubbell JA. Tenascin C promiscuously binds growth factors via its fifth fibronectin type III-like domain. *PLoS ONE.* (2013) 8:e62076. doi: 10.1371/journal.pone.0062076
98. Mercado-Gomez O, Landgrave-Gomez J, Arriaga-Avila V, Nebreda-Corona A, Guevara-Guzman R. Role of TGF-beta signaling pathway on Tenascin C protein upregulation in a pilocarpine seizure model. *Epilepsy Res.* (2014) 108:1694–704. doi: 10.1016/j.eplepsyres.2014.09.019
99. Tezel G, Li LY, Patil RV, Wax MB. TNF-alpha and TNF-alpha receptor-1 in the retina of normal and glaucomatous eyes. *Invest Ophthalmol Vis Sci.* (2001) 42:1787–94.
100. Kitaoka Y, Kitaoka Y, Kwong JM, Ross-Cisneros FN, Wang J, Tsai RK, et al. TNF-alpha-induced optic nerve degeneration and nuclear factor-kappaB p65. *Invest Ophthalmol Vis Sci.* (2006) 47:1448–57. doi: 10.1167/iovs.05-0299
101. Nakazawa T, Nakazawa C, Matsubara A, Noda K, Hisatomi T, She H, et al. Tumor necrosis factor-alpha mediates oligodendrocyte death and delayed retinal ganglion cell loss in a mouse model of glaucoma. *J Neurosci.* (2006) 26:12633–41. doi: 10.1523/JNEUROSCI.2801-06.2006
102. Cueva Vargas JL, Osswald IK, Unsain N, Arousseau MR, Barker PA, Bowie D, et al. Soluble tumor necrosis factor alpha promotes retinal ganglion cell death in glaucoma via calcium-permeable AMPA receptor activation. *J Neurosci.* (2015) 35:12088–102. doi: 10.1523/JNEUROSCI.1273-15.2015
103. Gregory MS, Hackett CG, Abernathy EF, Lee KS, Saff RR, Hohlbaum AM, et al. Opposing roles for membrane bound and soluble Fas ligand in glaucoma-associated retinal ganglion cell death. *PLoS ONE.* (2011) 6:e17659. doi: 10.1371/journal.pone.0017659
104. Krishnan A, Kocab AJ, Zacks DN, Marshak-Rothstein A, Gregory-Ksander M. A small peptide antagonist of the Fas receptor inhibits neuroinflammation and prevents axon degeneration and retinal ganglion cell death in an inducible mouse model of glaucoma. *J Neuroinflammation.* (2019) 16:184. doi: 10.1186/s12974-019-1576-3
105. Mac Nair CE, Fernandes KA, Schlamp CL, Libby RT, Nickells RW. Tumor necrosis factor alpha has an early protective effect on retinal ganglion cells after optic nerve crush. *J Neuroinflammation.* (2014) 11:194. doi: 10.1186/s12974-014-0194-3
106. Liu W, Tang Y, Feng J. Cross talk between activation of microglia and astrocytes in pathological conditions in the central nervous system. *Life Sci.* (2011) 89:141–6. doi: 10.1016/j.lfs.2011.05.011
107. Pekny M, Pekna M. Astrocyte reactivity and reactive astrogliosis: costs and benefits. *Physiol Rev.* (2014) 94:1077–98. doi: 10.1152/physrev.00041.2013
108. Norden DM, Trojanowski PJ, Villanueva E, Navarro E, Godbout JP. Sequential activation of microglia and astrocyte cytokine expression precedes increased Iba-1 or GFAP immunoreactivity following systemic immune challenge. *Glia.* (2016) 64:300–16. doi: 10.1002/glia.22930
109. Block ML, Zecca L, Hong JS. Microglia-mediated neurotoxicity: uncovering the molecular mechanisms. *Nat Rev Neurosci.* (2007) 8:57–69. doi: 10.1038/nrn2038
110. Tang Y, Le W. Differential Roles of M1 and M2 Microglia in Neurodegenerative Diseases. *Mol Neurobiol.* (2016) 53:1181–94. doi: 10.1007/s12035-014-9070-5
111. Claycomb KI, Winokur PN, Johnson KM, Nicaise AM, Giampetruzzi AW, Sacino AV, et al. Aberrant production of tenascin-C in globoid cell leukodystrophy alters psychosine-induced microglial functions. *J Neuropathol Exp Neurol.* (2014) 73:964–74. doi: 10.1097/NEN.000000000000117
112. Jack CS, Arbour N, Manusow J, Montgrain V, Blain M, Mccrea E, et al. TLR signaling tailors innate immune responses in human microglia and astrocytes. *J Immunol.* (2005) 175:4320–30. doi: 10.4049/jimmunol.175.7.4320
113. Rosenberger K, Derkow K, Dembny P, Kruger C, Schott E, Lehnardt S. The impact of single and pairwise Toll-like receptor activation on neuroinflammation and neurodegeneration. *J Neuroinflammation.* (2014) 11:166. doi: 10.1186/s12974-014-0166-7
114. Midwood K, Sacre S, Piccinini AM, Inglis J, Trebaul A, Chan E, et al. Tenascin-C is an endogenous activator of Toll-like receptor 4 that is essential for maintaining inflammation in arthritic joint disease. *Nat Med.* (2009) 15:774–80. doi: 10.1038/nm.1987
115. Zuliani-Alvarez L, Marzeda AM, Deligne C, Schwenzer A, Mccann FE, Marsden BD, et al. Mapping tenascin-C interaction with toll-like receptor 4 reveals a new subset of endogenous inflammatory triggers. *Nat Commun.* (2017) 8:1595. doi: 10.1038/s41467-017-01718-7
116. Parameswaran N, Patial S. Tumor necrosis factor-alpha signaling in macrophages. *Crit Rev Eukaryot Gene Expr.* (2010) 20:87–103. doi: 10.1615/CritRevEukaryotGeneExpr.v20.i2.10
117. Giblin SP, Schwenzer A, Midwood KS. Alternative splicing controls cell lineage-specific responses to endogenous innate immune triggers within the extracellular matrix. *Matrix Biol.* (2020). doi: 10.1016/j.matbio.2020.06.003
118. Paschalis EI, Lei F, Zhou C, Kapoulea V, Thanos A, Dana R, et al. The role of microglia and peripheral monocytes in retinal damage after corneal chemical injury. *Am J Pathol.* (2018) 188:1580–96. doi: 10.1016/j.ajpath.2018.03.005
119. Midwood KS, Chiquet M, Tucker RP, Orend G. Tenascin-C at a glance. *J Cell Sci.* (2016) 129:4321–7. doi: 10.1242/jcs.190546
120. Marzeda AM, Midwood KS. Internal affairs: Tenascin-C as a clinically relevant, endogenous driver of innate immunity. *J Histochem Cytochem.* (2018) 66:289–304. doi: 10.1369/0022155418757443
121. Roberts AL, Mavlyutov TA, Perlmutter TE, Curry SM, Harris SL, Chauhan AK, et al. Fibronectin extra domain A (FN-EDA) elevates intraocular pressure through Toll-like receptor 4 signaling. *Sci Rep.* (2020) 10:9815. doi: 10.1038/s41598-020-66756-6
122. Wiemann S, Reinhard J, Reinehr S, Cibir Z, Joachim SC, Faissner A. Loss of extracellular matrix molecule tenascin-C leads to absence of reactive gliosis and promotes anti-inflammatory cytokine expression in an autoimmune glaucoma model. *bioRxiv.* (2020). doi: 10.1101/2020.04.28.064758

Conflict of Interest: The authors declare that the research was conducted in the absence of any commercial or financial relationships that could be construed as a potential conflict of interest.

Copyright © 2020 Wiemann, Reinhard, Reinehr, Cibir, Joachim and Faissner. This is an open-access article distributed under the terms of the Creative Commons Attribution License (CC BY). The use, distribution or reproduction in other forums is permitted, provided the original author(s) and the copyright owner(s) are credited and that the original publication in this journal is cited, in accordance with accepted academic practice. No use, distribution or reproduction is permitted which does not comply with these terms.